Dipole strength distributions in the stable Ba isotopes $^{134-138}$Ba: A study in the mass region of a nuclear shape transition

M. Scheck,[1] H. von Garrel,[1] N. Tsoneva,[2,*] D. Belic,[1,†] P. von Brentano,[3] C. Fransen,[3] A. Gade,[3,‡] J. Jolie,[3] U. Kneissl,[1] C. Kohstall,[1] A. Linnemann,[3] A. Nord,[1,†] N. Pietralla,[3,§] H. H. Pitz,[1] F. Stedile,[1] C. Stoyanov,[4] and V. Werner[3]

[1]*Institut für Strahlenphysik, Universität Stuttgart, D-70569 Stuttgart, Germany*

[2]*Institut für Theor. Physik, Universität Giessen, D-35392 Giessen, Germany*

[3]*Institut für Kernphysik, Universität zu Köln, D-50937 Köln, Germany*

[4]*Institute for Nuclear Research and Nuclear Energy, 1784 Sofia, Bulgaria*

(Received 21 January 2004; published 29 October 2004)

The low-lying dipole strength distributions in the odd-mass isotopes ^{135,137}Ba were studied in nuclear resonance fluorescence experiments (NRF) performed at the Stuttgart Dynamitron facility using bremsstrahlung beams with end point energies of 4.1, 3.1, and 2.5 MeV. Numerous excited states, most of them unknown so far, were observed in the excitation energy range up to 4 MeV. Detailed spectroscopic information has been obtained on excitation energies, decay widths, decay branching ratios, and transition probabilities. The results for ^{137}Ba are compared with calculations in the framework of the Quasiparticle-Phonon Model. The new data for ^{135,137}Ba complete the systematics of low-lying dipole excitations as observed for the even Ba isotopes ^{134,136,138}Ba in previous NRF experiments in Stuttgart. The complete systematics within the Ba isotopic chain, exhibiting a nuclear shape transition, is discussed with respect to $E1$ two-phonon excitations, $M1$ scissors mode excitations, and in regard to the new critical point symmetries.

DOI: 10.1103/PhysRevC.70.044319 PACS number(s): 25.20.Dc, 21.10.Re, 23.20.Lv, 27.60.+j

I. INTRODUCTION AND MOTIVATION

Systematic investigations of nuclei within isotopic chains undergoing a shape or phase transition are of particular current interest in nuclear structure physics. In the framework of algebraic models the dynamical symmetry limits U(5), SU(3), and O(6) correspond to spherical, axially deformed, and γ-soft nuclear shapes, respectively. Recently, Iachello [1–3] proposed three new so-called critical point symmetries E(5), X(5), and Y(5) which apply for nuclei at the critical points of phase transitions from spherical vibrators to deformed γ-soft nuclei, to axially symmetric deformed rotors, and from axially symmetric to rigidly triaxial rotors, respectively. Experimental manifestations of these symmetries have already been found in ^{134}Ba [E(5)] [4], in ^{152}Sm, ^{150}Nd [X(5)] [5–7], and possibly in ^{166,168}Er [3]. Of special interest are nuclei at the critical point of phase transitions since drastic changes in the nuclear structure and hence in the various experimental observables are there to be expected such as excitation schemes, $B(E2)$ and $B(M1)$ transition rates. In this work we want to investigate the influence of a phase shape transition on low-lying dipole strength distributions.

A first hint for such effects in dipole strength distributions is the sudden onset of a deformation splitting of the higher-lying electric giant dipole resonance (GDR), centered at about 15 MeV, as observed in systematic studies of the ^{144,148,150,152,154}Sm and ^{142,143,144,145,146,148,150}Nd isotopes [8,9]. The splitting appears abruptly for ^{152}Sm and ^{150}Nd, which are just the nuclei that show the spectral properties predicted within the X(5) picture [5,6]. Also, recent systematic IBM calculations [10] of level energies, $B(E2)$ values, and two-neutron separation energies of nuclei within isotopic chains of rare earth nuclei manifest ^{148}Nd/^{150}Nd and ^{150}Sm/^{152}Sm as best candidates for the shape transition from spherical vibrators to axially deformed rotors.

It is well known that photon scattering [11], nuclear resonance fluorescence (NRF), represents the most sensitive tool to study low-lying dipole modes in heavy nuclei. Examples of rather collective, low-lying excitations, systematically studied in recent years, are the $M1$ scissors mode [12,13] in deformed nuclei ([11,14–17], and references therein) and $E1$ two-phonon excitations in spherical nuclei near shell closures (see compilation in Ref. [18]). The dipole strength distributions of stable nuclei within the Sm [19,20] and Nd [21–23] isotopic chains that exhibit a transition from the spherical $N=82$ isotones to axially deformed rotors have been systematically investigated in previous NRF experiments. In these measurements a concentration and jump of the total $M1$ scissors mode strength for ^{152}Sm [19,20] and ^{150}Nd [21–23] was observed in accordance with the other signatures for shape transitions discussed above.

Another interesting shape transition occurring in the mass region around $N=82$ is the transition from spherical to γ-soft nuclei. Favorable cases to study the dipole strength distributions in such nuclei by NRF experiments represent the Xe and Ba isotopic chains. The latter contains seven stable isotopes, starting from a magic, spherical vibrator (^{138}Ba, $N=82$) and ending with deformed, γ-soft nuclei around

*Also at: Institute for Nuclear Research and Nuclear Energy, 1784 Sofia, Bulgaria.

†Present address: Agilent Technologies, D-71034 Böblingen, Germany.

‡Present address: NSCL, Michigan State University, East Lansing, MI 48824, USA.

§Present address: Department of Physics and Astronomy, State University of New York, Stony Brook, NY 11794-3800, USA.

TABLE I. Beam parameters and measuring times.

Isotope	Endpoint energy (MeV)	Electron current (μA)	Measuring time (h)
^{134}Ba	4.1	220	696[a]
	4.1	180	64[b]
^{135}Ba	4.1	210	146
	2.5	320	88
^{136}Ba	4.1	230	120
	2.7	360	81
^{137}Ba	4.1	260	94
	3.1	300	105
^{138}Ba	4.1	200	60

[a]Polarization measurements.
[b]Angular distribution measurements.

^{130,132}Ba. The γ-soft character of nuclei in the $A \approx 130$ mass region has been well established [24]. Of special interest is the isotope ^{134}Ba which was proposed as one of the E(5) candidates [4].

In the present paper the results from our previous NRF studies of ^{134}Ba [25], ^{136}Ba [26], and ^{138}Ba [27] are summarized, discussed in view of the new dynamical symmetries and completed by comprehensive new data observed for the odd-mass Ba isotopes ^{135,137}Ba in NRF experiments performed at the Stuttgart photon scattering facility. The dipole strength distributions in these isotopes give information on the fragmentation of the electric and magnetic dipole modes (scissors mode and two-phonon excitations, respectively). Furthermore, these low-lying dipole strength distributions are of interest because they may explain the surprisingly strong population of the long-lived $h_{11/2}$ isomers in ^{135,137}Ba observed in low-energy (γ, γ')-reactions [28–31].

The outline of the paper is as follows: After the Introduction, the basic formalism describing NRF experiments is summarized in Sec. II and some experimental details are briefly given in Sec. III. The new results for the odd-mass isotopes ^{137,135}Ba are presented in Sec. IV. The last section, Sec. V, deals with the discussion of the results. Five topics are covered in more detail in the subsections A–E: The systematics of the dipole strength distributions in all investigated Ba isotopes (A), the comparison of the data for ^{137}Ba with recent QPM calculations (B), $M1$ and $E1$ excitations and their fragmentation in the odd-mass isotopes (C and D), and the systematics of the dipole strength distributions in view of the new critical point symmetries (E).

II. NUCLEAR RESONANCE FLUORESCENCE

Photon scattering experiments provide model-independent spectroscopic information. Precise excitation energies E_x and integrated elastic scattering cross sections $I_{S,0}$, which are proportional to width ratios Γ_0^2/Γ, can directly be determined from the spectra of scattered photons. Ground-state transition widths Γ_0, and total widths Γ of the excited states can be extracted from the scattering intensities and from the observed decay branchings. Reduced excitation probabilities $B(E1)\uparrow$, $B(M1)\uparrow$, $B(E2)\uparrow$, or lifetimes τ can be deduced from these quantities. Spins and parities of the photoexcited states can be determined in the favorable cases of even–even nuclei by measurements of angular distributions and polarization observables. Unfortunately, in the case of odd-mass target nuclei, the angular distributions of the scattered photons are rather isotropic. Therefore, generally no unambiguous spin assignments to the photoexcited states are possible, particularly not for isotopes with large ground-state spins. Furthermore, no parity assignments are possible by linear polarization measurements, since the nearly vanishing anisotropy in the angular distributions leads to rather low degrees of polarization of the scattered photons. In spite of generally unknown spins and parities, the observed photon scattering

TABLE II. Target compositions and specifications.

Isotope	Composition	Enrichment (%)	Total masses (mg) Target	^{27}Al	LiF	Major impurities (%)
^{134}Ba	$BaCO_3$	82.1	1880	1206		averaged
^{134}Ba	$BaCO_3$	85.5	485			^{135}Ba(4.1), ^{136}Ba(1.8),
^{134}Ba	$Ba(NO_3)_2$	86.2	2608			^{137}Ba(1.7), ^{138}Ba(7.9),
^{134}Ba	$Ba(NO_3)_2$	86.2	1464	213		^{135}Ba (3.5), ^{136}Ba (1.7) ^{137}Ba (1.6), ^{138}Ba (6.9)
^{135}Ba	$BaCO_3$	66.3	3567	1010		^{134}Ba (8.5), ^{136}Ba (8.9) ^{137}Ba (5.0), ^{138}Ba (11.4)
^{136}Ba	$BaCO_3$	92.8	1076	1016	1098	^{135}Ba (1.0.), ^{137}Ba (1.8) ^{138}Ba (4.3)
^{136}Ba	$BaCO_3$	92.8	1029	508		^{135}Ba (1.0.), ^{137}Ba (1.8) ^{138}Ba (4.3)
^{137}Ba	$BaCO_3$	82.2	4317	1013		^{138}Ba (17.5)
^{137}Ba	$BaCO_3$	82.2	4317	755		^{138}Ba (17.5)
^{138}Ba	$BaCO_3$	99	1043	215		-

cross sections enable one to determine the quantity

$$g \cdot \Gamma_0^{\mathrm{red}} = g \cdot \frac{\Gamma_0}{E_x^3}, \tag{1}$$

which is proportional to the reduced dipole excitation probabilities $B(E1)\uparrow$ or $B(M1)\uparrow$. Here, Γ_0 is the ground-state transition width, $g=(2J+1)/(2J_0+1)$ the so-called statistical spin factor, and E_x the excitation energy. The following numerical relations are useful:

$$B(E1)\uparrow = 0.955 \cdot g \cdot \Gamma_0^{\mathrm{red}}\,[10^{-3}e^2\mathrm{fm}^2], \tag{2}$$

$$B(M1)\uparrow = 0.0864 \cdot g \cdot \Gamma_0^{\mathrm{red}}\,[\mu_N^2], \tag{3}$$

where the excitation energies E_x should be taken in (MeV) and the ground-state transition widths Γ_0 in (meV).

In the case of decay branchings of the photoexcited states to lower-lying excited states the branching ratio $R_{\mathrm{expt.}}$ relative to the ground-state decay can be measured, defined by

$$R_{\mathrm{expt.}} = \frac{B(\Pi L;\ J \rightarrow J_f)}{B(\Pi L;\ J \rightarrow J_0)} = \frac{\Gamma_f}{\Gamma_0} \cdot \frac{E_{\gamma J_0}^3}{E_{\gamma J_f}^3}. \tag{4}$$

Since no coincidence experiments are feasible at present NRF setups, possible decays of the photoexcited states to low-lying excited states ("inelastic transitions") were searched for by applying the Ritz combination rule:

$$E_i - (E_x - E_f) \leqslant |\Delta E|, \tag{5}$$

where E_x, E_i, and E_f are the level excitation energy, the energy of a possible inelastic transition and of the final low-lying excited state, respectively. For the assignments of inelastic transitions, a limit of $\Delta E = \pm 1$ keV was chosen, which corresponds to a realistic value of the total uncertainties in the needed energy determinations.

The formalism describing NRF experiments is summarized in more detail in previous review articles [11,32].

III. EXPERIMENTAL DETAILS

The present NRF experiments on ^{135,137}Ba and the previously published studies of the even–even Ba isotopes [25–27] were performed at the well-established Stuttgart bremsstrahlung facility [11]. Measurements using bremsstrahlung end point energies of 4.1, 3.1, and 2.5 MeV were carried out to achieve an optimal sensitivity over a broad range of excitation energies and to enable the detection of weaker decay branching ratios. The dc electron currents used in the present experiments had to be limited to about 250 μA, due to the thermal capacity of the radiator target of about 1 kW. In Table I beam parameters and measuring times of the NRF experiments on ^{134,135,136,137,138}Ba are summarized. For all experiments isotopically enriched targets were available (see Table II).

The scattered photons were detected by three high-resolution Ge(HP) γ-ray spectrometers installed at angles of about 90°, 127°, and 150° with respect to the incoming bremsstrahlung beam. Each of the detectors had an efficiency of about 100% relative to a standard 7.6 cm$\times$7.6 cm NaI(Tl) detector. The energy resolutions were typically about 2 keV at a photon energy of 1.3 MeV and about 3 keV at 3 MeV. The detector at 127° was additionally surrounded by a BGO anti-Compton shield to improve its response function. With this arrangement the peak-to-background ratio could be improved by a factor of about 2.

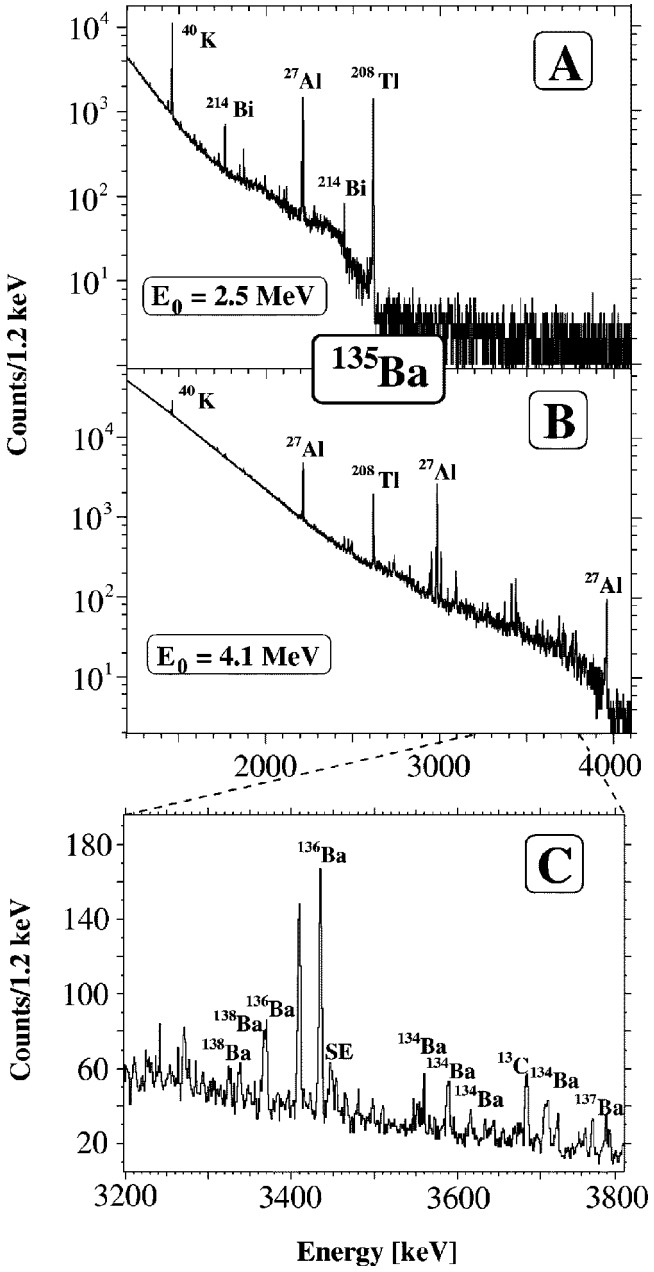

FIG. 1. Spectra of photons scattered off ^{135}Ba, measured at a scattering angle of 127° using bremsstrahlung beams of end point energies of 2.5 MeV [upper part (A)] and 4.1 MeV [lower part (B)], respectively. Calibration lines (^{27}Al), and background lines (mother activities: ^{40}K, and ^{208}Tl) are marked. Please note the logarithmic ordinate scale. Part (C) shows in a linear scale an expanded portion (3.2–3.8 MeV) of spectrum (B). Labeled peaks stem from strong excitations in the even–even isotopes ^{134,136,138}Ba which were contained as impurities in the targets. The peak marked by "SE" corresponds to a single escape peak.

TABLE III. Numerical results for dipole excitations in ^{135}Ba: Excitation energies E_x, total elastic scattering cross sections $I_{S,0}$, the product of the statistical factor g times the ground-state widths Γ_0, respectively, the reduced ground-state widths Γ_0^{red}, the branching ratios Γ_0/Γ, and the reduced excitation strengths $B(M1)\uparrow$ and/or $B(E1)\uparrow$. In cases of unknown parities the reduced excitation strengths are given in parentheses.

E_x (keV)	$I_{S,0}$ (eV b)	$g\Gamma_0$ (meV)	Γ_0/Γ	$g\Gamma_0^{\mathrm{red}}$ (meV/MeV^3)	$B(E1)\uparrow$ ($10^{-3}e^2$fm^2)	$B(M1)\uparrow$ μ_N^2
980[a]	9.01(64)	2.78(51)	0.81(9)[c]	2.96(54)		0.255(47)
1214[a]	1.94(30)	0.92(21)	0.81(6)	0.51(12)	[0.49(11)]	[0.044(10)]
1872[a]	3.54(27)	5.9(16)	0.55(11)[c]	0.89(25)	[0.85(24)]	[0.077(21)]
1942[b]	0.56(15)	2.41(63)	0.23(10)[c]	0.33(9)		0.028(7)
1965[a]	0.70(17)	2.5(17)	0.28(13)[c]	0.33(23)		0.028(20)
1991[b]	1.10(18)	4.10(69)	0.28(14)[c]	0.52(9)	[0.50(8)]	[0.045(8)]
2077[a]	1.57(18)	4.5(13)	0.39(7)[c]	0.50(15)	0.48(14)	
2283	0.98(22)	1.33(30)	1	0.11(3)	[0.11(2)]	[0.010(2)]
2334	1.25(22)	1.77(32)	1	0.14(3)	[0.13(2)]	[0.012(2)]
2420	1.19(21)	1.81(33)	1	0.13(2)	[0.12(2)]	[0.011(2)]
2440	1.43(22)	2.22(34)	1	0.15(2)	[0.15(2)]	[0.013(2)]
2447[d]	1.79(24)	3.87(84)	0.72(6)[c]	0.26(6)	[0.25(6)]	[0.023(5)]
2478	1.28(21)	2.05(33)	1	0.14(2)	[0.13(2)]	[0.012(2)]
2485	1.67(23)	2.69(37)	1	0.18(2)	[0.17(2)]	[0.015(2)]
2496	1.17(21)	1.90(34)	1	0.12(2)	[0.12(2)]	[0.011(2)]
2602[d]	0.95(18)	1.68(32)	1	0.10(2)	[0.09(2)]	[0.008(2)]
2621	1.99(23)	3.56(41)	1	0.20(2)	[0.19(2)]	[0.017(2)]
2638	1.29(21)	2.33(38)	1	0.13(2)	[0.12(2)]	[0.011(2)]
2658	1.08(20)	2.48(93)	0.80(15)[c]	0.13(5)	[0.13(5)]	[0.011(4)]
2708[d]	1.18(24)	2.26(45)	1	0.11(2)	[0.11(2)]	[0.010(2)]
2710	0.88(22)	10.53(91)	0.16(2)	0.49(5)	[0.47(5)]	[0.043(4)]
2730	1.98(24)	6.1(14)	0.63(7)[c]	0.30(7)	[0.29(7)]	[0.026(6)]
2781	1.43(21)	2.88(42)	1	0.13(2)	[0.13(2)]	[0.012(2)]
2872[d]	1.38(20)	5.55(68)	0.54(7)	0.23(3)	[0.22(3)]	[0.020(3)]
2947	10.48(81)	23.7(18)	1	0.93(7)	[0.89(7)]	[0.080(6)]
3092[d]	4.58(50)	18.3(16)	0.63(6)	0.62(6)	[0.59(5)]	[0.053(5)]
3111	1.03(22)	2.60(55)	1	0.09(2)	[0.08(2)]	[0.008(2)]
3122	1.05(24)	2.67(61)	1	0.09(2)	[0.08(2)]	[0.008(2)]
3126	0.98(22)	8.2(10)	0.31(4)	0.27(3)	[0.26(3)]	[0.023(3)]
3148[d]	1.51(23)	7.44(97)	0.52(7)	0.24(3)	[0.23(3)]	[0.021(3)]
3163[d]	0.60(19)	1.57(50)	1	0.05(2)	[0.05(2)]	[0.004(1)]
3182	1.37(21)	3.60(54)	1	0.11(2)	[0.11(2)]	[0.010(2)]
3196	1.04(21)	2.76(55)	1	0.09(2)	[0.08(2)]	[0.007(2)]
3272[d]	2.06(26)	11.6(12)	0.50(5)	0.33(4)	[0.32(3)]	[0.029(3)]
3324	0.81(19)	2.32(56)	1	0.06(2)	[0.06(2)]	[0.005(1)]
3410[d]	9.43(76)	33.4(24)	0.85(6)	0.84(6)	[0.81(6)]	[0.073(5)]
3415	0.91(24)	2.75(73)	1	0.07(2)	[0.07(2)]	[0.006(2)]
3422	0.92(21)	2.82(64)	1	0.07(2)	[0.07(2)]	[0.006(1)]
3454	1.80(27)	18.3(17)	0.31(3)	0.44(4)	[0.42(4)]	[0.038(3)]
3587	0.96(31)	3.2(10)	1	0.07(2)	[0.07(2)]	[0.006(2)]
3632	1.06(26)	3.65(91)	1	0.08(2)	[0.07(2)]	[0.007(2)]
3656	1.35(28)	10.8(17)	0.44(7)	0.22(4)	[0.21(3)]	[0.019(3)]
3696	1.25(29)	4.5(10)	1	0.09(2)	[0.08(2)]	[0.008(2)]
3708[d]	4.50(50)	29.6(32)	0.54(6)	0.58(6)	[0.55(6)]	[0.050(6)]
3720	3.56(42)	12.8(15)	1	0.25(3)	[0.24(3)]	[0.022(3)]

TABLE III. (*Continued.*)

E_x (keV)	$I_{S,0}$ (eV b)	$g\Gamma_0$ (meV)	Γ_0/Γ	$g\Gamma_0^{\mathrm{red}}$ (meV/MeV^3)	$B(E1)\uparrow$ ($10^{-3}e^2\mathrm{fm}^2$)	$B(M1)\uparrow$ μ_N^2
3753[d]	2.36(43)	8.7(16)	1	0.16(3)	[0.16(3)]	[0.014(3)]
3779[d]	3.02(52)	11.2(19)	1	0.21(4)	[0.20(3)]	[0.018(3)]
3813	1.87(52)	7.1(20)	1	0.13(4)	[0.12(3)]	[0.011(3)]
3881	2.29(47)	9.0(18)	1	0.15(3)	[0.15(3)]	[0.013(3)]

[a]Average values of data from measurements using various bremsstrahlung end point energies.
[b]Data from low-energy end point measurements only.
[c]Reference [35].
[d]Alternative assignments are possible, see subsequent tables.

The NRF measurements were complemented by photoactivation experiments to study the population of the low-lying $h_{11/2}$ isomers in ^{135,137}Ba by feeding from higher-lying photoexcited intermediate states. These results will be published in a forthcoming article [33].

IV. RESULTS

A. Results for ^{135}Ba(γ,γ')

Figure 1 shows the spectra of photons scattered off ^{135}Ba detected under a scattering angle of 127°. The spectrum depicted in the upper part (A) was measured using a bremsstrahlung beam of an end point energy of 2.5 MeV. In the middle part (B) the corresponding spectrum for an end point energy of 4.1 MeV is plotted. Both spectra are shown in logarithmic scales. The photon flux calibration lines (^{27}Al) and the background lines stemming from natural environmental activities (mother activities: ^{40}K, ^{214}Bi, and ^{208}Tl) are marked. All other peaks are ascribed to excitations in Ba isotopes, mostly to transitions in ^{135}Ba. The comparison between both spectra clearly documents the considerably enhanced peak-to-background ratio at low energies in the upper spectrum taken with a reduced end point energy of 2.5 MeV. This allows a better detection and identification of inelastic transitions and hence the measurement of weaker decay branching ratios to lower-lying excited states with improved sensitivity. In the lower part (C), an expanded portion of the spectrum (B) is shown in a linear scale to demonstrate the quality of the obtained spectra and the pronounced fragmentation of the dipole strengths, but also to exhibit the difficulties due to the somewhat low enrichment of the target (66.3% of ^{135}Ba). The labeled peaks stem from strong transitions in the even–even Ba isotopes ^{134,136,138}Ba, which were the main impurities (see Table II). These excitations have to be known and must not be considered to avoid misinterpretations.

The numerical results obtained for observed dipole excitations in ^{135}Ba are summarized in Table III. Given are the excitation energies E_x, the total elastic scattering cross sections $I_{S,0}$, the product of the statistical factor g times the ground-state widths Γ_0, the respective reduced ground-state widths Γ_0^{red}, and the branching ratios Γ_0/Γ. Since no direct parity measurements could be carried out, in the last two columns the reduced excitation widths $B(E1)\uparrow$ and $B(M1)\uparrow$ are given for both multipolarities $E1$ and $M1$. Only for dipole transitions of known parity is a definite reduced excitation probability $B(E1)\uparrow$ or $B(M1)\uparrow$ quoted. Whereas about half of the low-lying states up to an excitation energy of about 2.9 MeV were known from previous (n,γ) experiments [34], the higher-lying states were observed for the first time.

The isotope ^{135}Ba has a ground-state spin $J_0^\pi = 3/2^+$. Therefore, by photoexcitations via dipole transitions, levels with spins $1/2$, $3/2$, and $5/2$ can be reached, which then can populate, besides the ground state, lower-lying excited states with spins $1/2-7/2$. Due to the structure of ^{135}Ba, which has three neutron holes in the $N=82$ shell, besides the $h_{11/2}$ intruder isomer at 268 keV, eight low-spin levels exist below 1 MeV, which can be fed from the higher-lying photoexcited states or from the capture state in thermal neutron (n,γ) reactions [34]. In Fig. 2 the low-energy excitation scheme of ^{135}Ba is depicted and compared to the much simpler level scheme of ^{137}Ba. In the present NRF experiments, decay

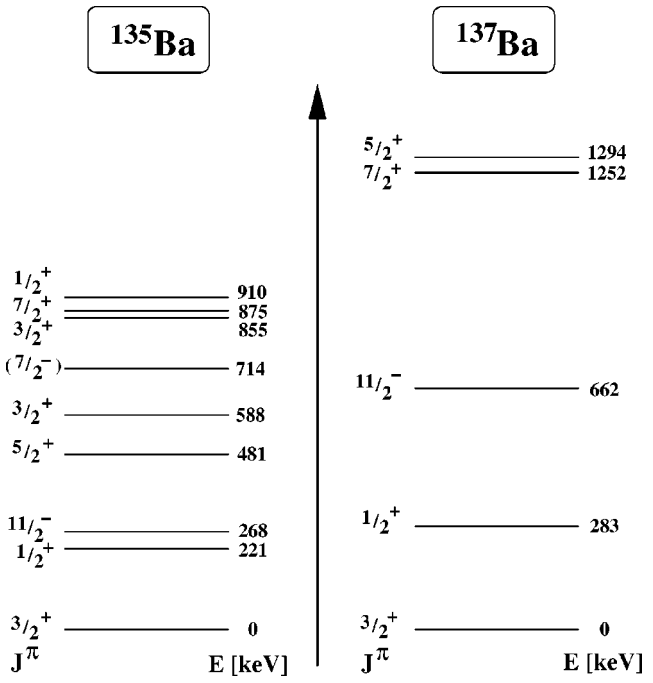

FIG. 2. Simplified low-energy excitation schemes of ^{135}Ba and ^{137}Ba.

TABLE IV. Decay branchings of photoexcited states in ^{135}Ba. The level energies given are E_x, the excitation energies E_{f_i} and E_{f_j} of the fed lower-lying states, and the corresponding decay branchings Γ_i/Γ_0 and Γ_j/Γ_0, respectively. Alternative assignments due to ambiguous, possible branchings are proposed in the same nomenclature as in Tables III and V.

Alternative	E^x (keV)	E_{f_i} (keV)	Γ_i/Γ_0	E_{f_j} (keV)	Γ_j/Γ_0
	2710	221	5.25(25)		
	2872	221	0.87(30)		
	3092	714	0.60(16)		
	3126	480.5	2.27(85)		
	3148	480.5	0.91(33)		
	3272	588	1.01(30)		
	3410	221	0.17(4)		
	3454	480.5	2.27(59)		
	3656	588	1.30(57)		
	3708	910	0.83(26)		
1	3092	221	0.37(9)	714	0.60(16)
2	2667	221	2.47(88)		
3a	3779	588	1.13(39)	980	1.71(64)
3b	3190	480.5	2.66(76)	588	1.33(48)
	3708	910	0.83(26)		
4	3163	480.5	3.1(15)		
	3753	480.5	2.01(62)		

branchings to six of these levels could be detected. The excitation energies E_x of the levels exhibiting decays to lower-lying excited states (in addition to the ground state), the energies E_i of the fed levels, and the corresponding branching ratios Γ_i/Γ_0 are summarized in Table IV.

Unfortunately, ambiguities in the assignments of photoexcited levels from the observed transitions cannot be avoided due to the pronounced fragmentation of the strength and numerous decay branchings when simply applying the Ritz combination technique without coincidence measurements. Therefore, possible alternative level assignments are given in Table V.

As already mentioned, spins could not be determined from the nearly isotropic angular distributions. Therefore, in general, the dipole character of the excitations was assumed with one exception, the $E2$ excitation of the known $7/2^+$

TABLE V. Alternative level assignments in ^{135}Ba due to ambiguous decay branchings, see Table IV. The quantities are the same as in Table III.

Alternative	E_x (keV)	$I_{S,0}$ (eV b)	$g\Gamma_0$ (meV)	Γ_0/Γ	$g\Gamma_0^{\mathrm{red}}$ (meV/MeV^3)	$B(E1)\uparrow$ ($10^{-3}e^2$fm^2)	$B(M1)\uparrow$ (μ_N^2)
1	2651	0.99(20)	1.81(37)	1	0.10(2)	[0.09(2)]	[0.008(2)]
	3092	4.58(50)	22.5(17)	0.51(4)	0.76(6)	[0.73(6)]	[0.066(5)]
2	2667	0.87(19)	5.62(65)	0.29(3)	0.30(3)	[0.28(3)]	[0.026(3)]
	3148	1.51(23)	3.90(59)	1	0.13(2)	[0.12(2)]	[0.011(2)]
3a	2708	2.09(25)	3.99(47)	1	0.20(2)	[0.19(2)]	[0.017(2)]
	3410	9.43(76)	28.5(23)	1	0.72(6)	[0.69(6)]	[0.062(5)]
	3708	4.50(50)	16.1(18)	1	0.32(4)	[0.30(3)]	[0.027(3)]
	3779	3.02(52)	43.0(48)	0.26(3)	0.80(9)	[0.76(9)]	[0.069(8)]
3b	3190	1.24(21)	16.5(14)	0.20(2)	0.51(4)	[0.48(4)]	[0.044(4)]
	3410	9.43(76)	28.5(23)	1	0.72(6)	[0.69(6)]	[0.062(5)]
	3708	4.50(50)	29.6(32)	0.54(6)	0.58(6)	[0.55(6)]	[0.050(6)]
	3779	3.02(52)	11.2(19)	1	0.21(4)	[0.20(3)]	[0.018(3)]
4	3163	0.60(19)	6.38(95)	0.25(4)	0.20(3)	[0.19(3)]	[0.017(3)]
	3753	2.36(43)	26.1(27)	0.33(3)	0.49(5)	[0.47(5)]	[0.043(4)]

state at 874 keV (see Table VIII). The measured reduced transition probability $B(E2)\uparrow$ is in fair agreement with data from previous Coulomb-excitation experiments [38].

B. Results for ^{137}Ba(γ,γ')

In Fig. 3 the spectra of photons scattered from ^{137}Ba are shown as measured using bremsstrahlung beams with end point energies of 4.1 MeV (upper part) and 3.1 MeV (lower part). The labeling is identical to that of Fig. 1. Comparing the 4.1 MeV spectra of both isotopes, a less pronounced strength fragmentation can be stated for ^{137}Ba where two accumulations of peaks around 3.1 and 3.8 MeV, respectively, are clearly visible.

The numerical results from the present ^{137}Ba(γ,γ') study are summarized in Table VI. The same quantities are given as in the corresponding Table III. Besides the state at 1892 keV, all observed photoexcited states below 2.1 MeV were also reported from previous neutron-induced reactions [(n,γ) and $(n,n'\gamma)$] [36]. All higher-lying states were observed for the first time.

Just as ^{135}Ba, ^{137}Ba has a ground-state spin of $J_0^\pi = 3/2^+$ ($\nu 2d_{3/2}$ hole). However, in contrast to ^{135}Ba, in ^{137}Ba below about 1 MeV besides the $11/2^-$ isomer at 662 keV ($h_{11/2}$ intruder) only one low-lying level exists at 283 keV with spin $J^\pi = 1/2^+$ ($\nu 3s_{1/2}$ hole) (see Fig. 2) as expected from the simple structure with one neutron hole apart from the closed $N=82$ shell. The other neutron-hole states, $2d_{5/2}$ and $1g_{7/2}$, as well as particle states, proton excitations, and states arising from the coupling of the neutron holes to excitations of the $N=82$ core lie at excitation energies above 1.2 MeV (see Ref. [36] and references therein). Therefore, and due to the less pronounced fragmentation of the dipole strength in ^{137}Ba, only two ambiguous level assignments are left in the analysis of the present data. The possible alternatives are given in Table VII. Decay branchings of the photoexcited states were observed in some cases exclusively to the 283 keV level. The corresponding branching ratios are included in Table VI.

For all observed excitations, a dipole character was assumed with the exception of the $E2$ excitation of the known $7/2^+$ level at 1252 keV. As in the case of ^{135}Ba, the observed reduced excitation strength $B(E2)\uparrow$ (see Table VIII) is in fair agreement with prior results from a Coulomb-excitation experiment [38].

V. DISCUSSION

A. Systematics of dipole strength distributions in ^{134,135,136,137,138}Ba

In Fig. 4 the observed spectra of photons scattered off the investigated isotopes ^{134,135,136,137,138}Ba are summarized and compared. The peaks stemming from the photon flux monitor ^{27}Al are marked as well as the transitions in the even–even isotopes ascribed to the expected two-phonon excitations (1^-) and the scissors mode (1^+). The spectrum for the closed-shell nucleus ^{138}Ba is dominated by the strong two-phonon excitation of the 1^- state at 4026 keV. The lower peaks correspond to $E2$ excitations (see Ref. [27]). The data

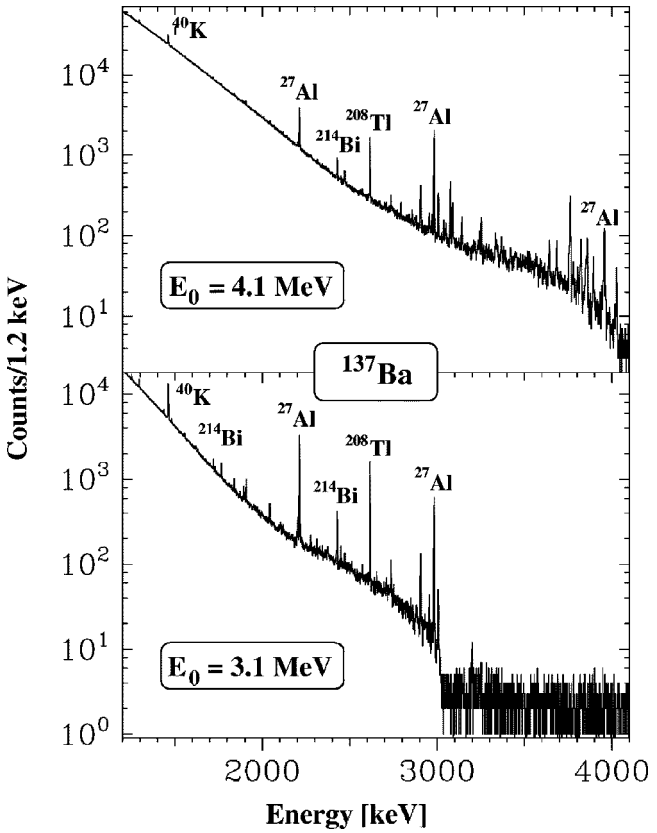

FIG. 3. Spectra of photons scattered off ^{137}Ba, measured at a scattering angle of 127° using bremsstrahlung beams of end point energies of 4.1 MeV (upper part) and 3.1 MeV (lower part), respectively. Calibration lines (^{27}Al), and background lines (mother activities: ^{40}K, ^{214}Bi, and ^{208}Tl) are marked. Please note the logarithmic ordinate scale.

on the observed $E2$ excitations in ^{138,136}Ba are summarized in Table IX. The corresponding $E1$ two-phonon excitations in ^{136,134}Ba are obviously shifted to lower energies as compared to ^{138}Ba and reduced in strength. The scissors-mode strength emerges in ^{136}Ba and increases as observed in ^{134}Ba. In addition, in ^{136}Ba a rather pure mixed-symmetry 2^+ state could be observed at 2129 keV [26]. In the odd-mass isotopes the dipole strength is more fragmented.

Figure 5 shows the dipole strength distributions extracted from the spectra of photons scattered off ^{134,135,136,137,138}Ba. The reduced ground-state transition widths $\Gamma_0^{\rm red}$ are plotted as a function of the excitation energy (for the even–even isotopes, where the spin factor g is known and equals 3) and the quantities $g\cdot\Gamma_0^{\rm red}$ for the odd-mass isotopes, since the spins of the photoexcited states could not be measured and hence the spin factor g is unknown. It should be recalled that the quantity $g\cdot\Gamma_0^{\rm red}$ is directly proportional to the reduced excitation probabilities $B(E1)\uparrow$ or $B(M1)\uparrow$, respectively [see Eqs. (2) and (3)]. Spin 1 states in the even–even isotopes with known parity are marked.

B. Comparison of the dipole strength distribution in ^{137}Ba with QPM calculations

Microscopic calculations of the dipole strength distribution were performed for the $N=81$ isotope ^{137}Ba with one

TABLE VI. Numerical results for dipole excitations in ^{137}Ba: Excitation energies E_x, total elastic scattering cross sections $I_{S,0}$, the product of the statistical factor g times the ground-state widths Γ_0, respectively, the reduced ground-state widths Γ_0^{red}, the branching ratios Γ_0/Γ, and the reduced excitation strengths $B(M1)\uparrow$ and/or $B(E1)\uparrow$. In cases of unknown parities the reduced excitation strengths are given in parentheses.

E_x (keV)	$I_{S,0}$ (eV b)	$g\Gamma_0$ (meV)	Γ_0/Γ	$g\Gamma_0^{\mathrm{red}}$ (meV/MeV^3)	$B(E1)\uparrow$ ($10^{-3}e^2$fm^2)	$B(M1)\uparrow$ (μ_N^2)
1294[a]	11.72(59)	5.10(26)	1	2.36(12)		0.204(10)
1464[a]	16.5(59)[d]	9.7(35)	0.95[c]	3.1(11)		0.261(94)
1481[a]	2.60(22)	2.47(21)	0.60[c]	0.76(7)		0.066(6)
1837[a]	2.16(17)	3.90(50)	0.49(2)	0.63(8)		0.054(7)
1892[a]	1.99(15)	1.85(14)	1	0.27(2)	[0.26(2)]	[0.024(2)]
1899[a]	1.26(14)	2.31(42)	0.51(4)	0.34(6)		0.029(5)
1907[a]	3.31(21)	4.67(49)	0.67(3)	0.67(7)		0.058(6)
2041[a]	2.17(16)	3.57(26)	0.66[c]	0.42(3)		0.036(3)
2117	1.00(20)	1.17(23)	1	0.12(2)	[0.12(2)]	[0.011(2)]
2311[a]	0.68(10)	0.95(13)	1	0.08(1)	[0.07(1)]	[0.007(1)]
2344[b]	0.58(12)	0.84(18)	1	0.07(1)	[0.06(1)]	[0.006(1)]
2373	0.89(16)	1.30(23)	1	0.10(2)	[0.09(2)]	[0.008(2)]
2427[a]	3.60(21)	5.52(32)	1	0.39(2)	[0.37(2)]	[0.033(2)]
2571[a]	0.73(9)	1.26(16)	1	0.07(1)	[0.07(1)]	[0.006(1)]
2653[b]	0.42(10)	0.77(19)	1	0.04(1)	[0.04(1)]	[0.004(1)]
2709	0.86(14)	1.64(28)	1	0.08(1)	[0.08(1)]	[0.007(1)]
2873	0.70(14)	1.50(29)	1	0.06(1)	0.06(1)	
2905[a]	5.58(31)	12.26(67)	1	0.50(3)	[0.48(3)]	[0.043(2)]
2954[a]	1.61(13)	5.33(74)	0.62(13)	0.21(3)	[0.20(3)]	[0.018(2)]
3037	2.02(20)	4.85(47)	1	0.17(2)	[0.17(2)]	[0.015(2)]
3074	11.22(82)	32.5(21)	0.85(11)	1.12(7)	[1.07(7)]	[0.097(6)]
3094	0.52(13)	1.28(32)	1	0.04(1)	[0.04(1)]	[0.004(1)]
3140	3.47(30)	13.83(96)	0.64(9)	0.45(3)	[0.43(3)]	[0.039(3)]
3251	2.77(27)	13.59(98)	0.56(8)	0.40(3)	[0.38(3)]	[0.034(3)]
3332	2.15(23)	12.24(93)	0.51(8)	0.33(3)	0.32(2)	
3383	0.82(16)	2.45(46)	1	0.06(1)	[0.06(1)]	[0.006(1)]
3453	0.94(17)	2.92(52)	1	0.07(1)	[0.07(1)]	[0.006(1)]
3473	0.84(16)	2.64(52)	1	0.06(1)	[0.06(1)]	[0.005(1)]
3525	1.22(19)	10.3(10)	0.38(7)	0.24(2)	[0.23(2)]	[0.020(2)]
3563[e]	1.19(21)	7.71(95)	0.51(13)	0.17(2)	[0.16(2)]	[0.015(2)]
3640	3.71(64)	12.8(22)	1	0.27(5)	0.25(4)	
3703	0.76(19)	10.5(13)	0.26(6)	0.21(3)	0.20(2)	
3761	33.5(26)	123.2(95)	1	2.32(18)	[2.21(17)]	[0.200(15)]
3778	4.12(41)	15.3(15)	1	0.28(3)	[0.27(3)]	[0.025(3)]
3802	2.83(34)	10.7(13)	1	0.19(2)	[0.19(2)]	[0.017(2)]
3822	10.64(92)	40.5(35)	1	0.73(6)	[0.69(6)]	[0.063(5)]
3846[e]	2.00(38)	7.7(15)	1	0.14(3)	[0.13(2)]	[0.012(2)]
3850	4.02(50)	25.0(25)	0.62(13)	0.44(4)	[0.42(4)]	[0.038(4)]
3857	12.3(11)	47.7(41)	1	0.83(7)	[0.79(7)]	[0.072(6)]
3894	7.98(77)	31.5(31)	1	0.53(5)	[0.51(5)]	[0.046(5)]
3940	3.03(43)	12.2(17)	1	0.20(3)	[0.19(3)]	[0.017(3)]
3981	2.12(45)	8.8(19)	1	0.14(3)	[0.13(3)]	[0.012(3)]

[a]Average values of data from measurements using various bremsstrahlung end point energies.
[b]Data from low-energy end point measurements only.
[c]Reference [37].
[d]Due to the overlap with the 1461 keV background line from ^{40}K an additional systematic error of 30% was added.
[e]Alternative assignments are possible, see Table VII.

TABLE VII. Alternative level assignments in ^{137}Ba due to ambiguous decay branchings, see Table VI. The quantities are the same as in table VI.

E_x (keV)	$I_{S,0}$ (eV b)	$g\Gamma_0$ (meV)	Γ_0/Γ	$g\Gamma_0^{\mathrm{red}}$ (meV/MeV^3)	$B(E1)\uparrow$ ($10^{-3}e^2$ fm^2)	$B(M1)\uparrow$ (μ_N^2)
3279	0.80(14)	2.23(40)	1	0.06(1)	[0.06(1)]	[0.006(1)]
3846	2.00(38)	16.4(21)	0.47(12)	0.29(4)	[0.28(4)]	[0.025(3)]

neutron hole in the closed $N=82$ shell within the framework of the quasiparticle-phonon model (QPM) [39]. The structure of ^{137}Ba has been calculated within this model. The application of the model in the case of odd-mass spherical nuclei is discussed in detail in Ref. [40]. Since in the present NRF experiments only $E1$, $E2$, and $M1$ transitions could be observed, our calculations are restricted to the states with $J^\pi = 1/2^\pm, 3/2^\pm, 5/2^\pm, 7/2^+$, and excitation energies up to 4.4 MeV.

Here, both the ground and excited states characterized by an angular momentum J and its projection M were described in terms of the wave function:

$$\Psi_\nu(JM) = C_J^\nu \Bigg\{ \alpha_{JM}^+ + \sum_{\lambda ij} D_j^{\lambda i}(J\nu)[\alpha_{jm}^+ Q_{\lambda\mu i}^+] + \sum_{\substack{\lambda_1 i_1 \lambda_2 i_2 \\ jI}} F_{jI}^{\lambda_1 i_1 \lambda_2 i_2}(J\nu) \times [\alpha_{jm}^+ (Q_{\lambda_1 \mu_1 i_1}^+ Q_{\lambda_2 \mu_2 i_2}^+)_{IM_1}]_{JM} \Bigg\} \Psi_0, \quad (6)$$

where α_{jm}^+ is the creation operator for a quasiparticle with shell quantum numbers $j \equiv (n,l,j)$ and m; $Q_{\lambda\mu i}^+$ is the phonon creation operator with the angular momentum λ, projection μ and the so-called QRPA root number i, the phonon index used to distinguish QRPA states of the same spin and parity but different energies; Ψ_0 is the ground state wave function of the neighboring even–even nucleus and ν stands for the number of the QRPA state of a given J^π. The coefficients C_J^ν, $D_j^{\lambda i}$, and $F_{jI}^{\lambda_1 i_1 \lambda_2 i_2}(J\nu)$ are the quasiparticle, quasiparticle $\otimes$ phonon and quasiparticle $\otimes$ two-phonon amplitudes for the ν state, respectively.

Most of the quasiparticle plus two-phonon components included in the wave function (6) have excitation energies higher than the studied energy range. Here only a limited number is considered. The numerical calculations are performed with the code PHOQUS modified according to Refs. [40] and [41]. To get the energy spectrum of the excited states and the wave function amplitudes we have solved a system of QRPA equations [40].

The QPM Hamiltonian includes mean field, pairing interaction, and separable multipole and spin–multipole interaction [39]. The mean field for protons and neutrons is defined as a Woods–Saxon potential with parameter sets given in Table X. The strength parameters of the quadrupole and octupole residual interaction are adjusted to reproduce the experimental values of the energies and reduced transition probabilities of low-lying collective states in the neighboring semimagic ^{138}Ba nucleus. The model space includes $\lambda^\pi = 1^\pm, 2^\pm, 3^\pm, 4^\pm, 5^-$ phonons in the wave function from Eq. (6). Several roots for each multipolarity are taken into account.

In the case of the E1 transitions, we have used effective charges $e_p = (N/A)e$ (for protons) and $e_n = -(Z/A)e$ (for neutrons) to separate the center of mass motion and "free" values for E2 transitions $e_p = e$ (for protons) and $e_n = 0$ (for neutrons). For the M1 transitions, the effective spin factor is $g^s = 0.8 g^s_{\mathrm{free}}$.

Because of the ground-state spin $3/2^+$, the $M1$ and $E2$ transitions correspond to the decay of the positive parity $J^\pi = 1/2^+$, $3/2^+$, $5/2^+$, and $7/2^+$ states. The calculated structure and corresponding values of ground-state decay widths $\Gamma(E2)$ and $\Gamma(M1)$, which are proportional to the corresponding $B(M1)$ or $B(E2)$ values, are presented in Table XI. The quasiparticle components dominate in the structure of a few excited states. Most of them are members of multiplets due to the coupling of quasiparticles mainly with the quadrupole excitations of the even–even core. When the structure of a state is dominated by the "quasiparticle $\otimes 2_1^+$" component, the corresponding $B(E2)$ transition probability is large. For example, the $3/2^+$ state at 1.687 MeV excitation energy is connected with the ground state via an $E2$ transition. The corresponding value of the transition probability is $B(E2) = 6.0$

TABLE VIII. $E2$ excitations in the odd-mass isotopes ^{135,137}Ba. Given are the excitation energies E_x, the integrated elastic scattering cross sections $I_{S,0}$, the products of the spin factor g times the corresponding ground-state decay widths Γ_0 and Γ_0^{red}, together with the decay branchings Γ_0/Γ and the reduced excitation probabilities $B(E2)\uparrow$.

Isotope	E_x (keV)	$I_{S,0}$ (eV b)	$g\Gamma_0$ (meV)	Γ_0/Γ	$g\Gamma_0^{\mathrm{red}}$ (meV/MeV^5)	$B(E2)\uparrow$ (e^2 fm^4)
^{135}Ba	874	4.52(54)	0.92(12)	0.98(0.01)[a]	1.80(23)	2238(290)
^{137}Ba	1252	8.88(45)	3.62(19)	1.00	1.18(6)	1467(75)

[a]Reference [35].

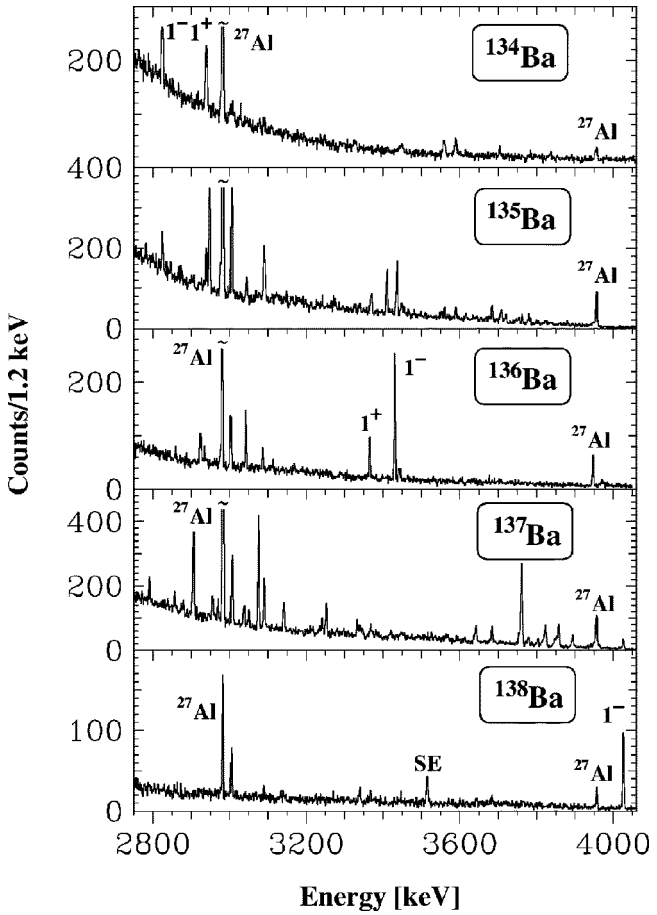

FIG. 4. Systematics of (γ, γ')-spectra observed for the stable Ba isotopes in NRF experiments using a bremsstrahlung end point energy of 4.1 MeV. Shown is the energy region where the $E1$ two-phonon and $M1$ scissors mode excitations are expected. Peaks attributed to these excitations in the even–even isotopes are marked by 1^- and 1^+. Peaks labeled by ^{27}Al belong to the aluminum photon flux calibration standard. SE labels a single escape peak.

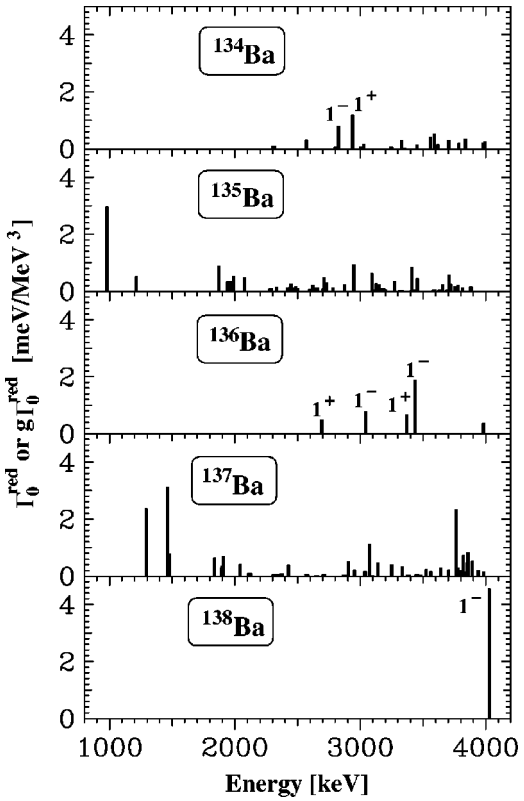

FIG. 5. Systematics of dipole strength distributions in the stable Ba isotopes observed in NRF experiments. Plotted are the reduced decay widths Γ_0^{red} (for even–even isotopes) or $g\Gamma_0^{\mathrm{red}}$ (for odd-mass isotopes), respectively, as a function of the excitation energy. For the even–even isotopes only dipole excitations are shown and assigned parities of states are given. The excitations in the odd-mass isotopes are most probably of dipole character, however, weak $E2$ excitations cannot be excluded.

TABLE IX. $E2$ excitations in the even–even Ba-isotopes ^{138,136}Ba. Given are the excitation energies E_x, the total scattering cross section $I_{S,0}$, the width ratios Γ_0^2/Γ and Γ_0/Γ together with the ground-state transition widths Γ_0 and the transition strengths $B(E2)\uparrow$. The branching ratios Γ_0/Γ were taken from literature [44]. For ^{134}Ba no $E2$ excitations could be detected.

Isotope	E_x (keV)	$I_{S,0}$ (eV b)	Γ_0^2/Γ (meV)	Γ_0/Γ	Γ_0 (meV)	$B(E2)\uparrow$ (e^2 fm^4)	Ref.
^{138}Ba	1436	23.1(25)	2.48(27)	1.00	2.48(27)	2535(275)	[27]
	2218	13.7(16)	3.51(41)	0.98	3.58(42)	415(50)	
	2640	4.2(12)	1.52(44)	0.87	1.75(51)	84(25)	
	3339	14.5(24)	8.4(14)	0.77(4)	10.9(19)	163(29)	
	3367	18.7(20)	11.0(12)	1.00	11.0(12)	158(18)	
	3643	15.7(28)	10.8(19)	0.63	17.1(30)	166(29)	
^{136}Ba	2129	4.25(0.24)	1.00(6)	0.32(4)	3.13(22)	446(31)	[26]
	3116	7.2(7)	3.6(4)	1.00	3.6(4)	76(9)	

TABLE X. Parameters of the Woods-Saxon potentials.

	r (fm)	V_0 (MeV)	κ (fm^2)	α (fm^{-1})
N	1.27	45.95	0.413	1.613
Z	1.31	53.435	0.349	1.538

$\times 10^2\ e^2$ fm^4. On the other hand, the state at 2.881 MeV with the same spin and parity $3/2^+$ is dominated in the structure by a "quasiparticle $\otimes$ phonon" component, $2d_{3/2}\otimes 2^+_5$. The 2^+_5 excitation of the even–even core is much less collective. This is the reason that the $E2$ transition connecting the latter with the ground state has $B(E2)=4.1\times 10^1\ e^2$ fm^4. The widths of both states have similar values because of the different excitation energies. For the widths $\Gamma(M1)$, such a regularity is not seen because the energy dependence of the width is not as sensitive as in the case of $E2$ transitions. The conclusion is that higher noncollective states, not only low-lying collective ones, give large contributions in the measured transitions.

The distribution of the low-lying dipole strength of ^{137}Ba could be studied via the structure of negative parity excitations. The low-lying $E1$ transitions in the neighboring ^{138}Ba nucleus have been successfully described by QPM calculations [42,43]. It was shown that the first 1^- state could be related to a quadrupole–octupole vibrational mode. This is the reason that in the present calculations of the low-lying dipole strength the two-phonon $[2^+_1\otimes 3^-_1]_{1^-}$ component is of greatest importance.

The structure of negative parity states $J^\pi=1/2^-$, $3/2^-$, $5/2^-$ of ^{137}Ba is calculated. The possible $[qp\otimes 2ph]$ configurations due to the coupling of the quasiparticles with the two-phonon $[2^+_1\otimes 3^-_1]_{1^-}$ component are taken into account. In particular we have included in the wave function (6) $[2d_{3/2}\otimes(2^+_1\otimes 3^-_1)]_{1/2^-,3/2^-,5/2^-}$, $[3s_{1/2}\otimes(2^+_1\otimes 3^-_1)]_{1/2^-,3/2^-}$, $[2d_{5/2}\otimes(2^+_1\otimes 3^-_1)]_{3/2^-,5/2^-}$, and $[2g_{7/2}\otimes(2^+_1\otimes 3^-_1)]_{5/2^-}$configurations. The $[2^+_1\otimes 3^-_1]_{1^-}$ component is fragmented over several $3/2^-$ states where the largest part of $[qp\otimes(2^+_1\otimes 3^-_1)_{1^-}]_{3/2^-}$ configurations is concentrated at 4.33 MeV (about 44.3% of the state vector, see Table XII). A considerable contribution of $[qp\otimes(2^+_1\otimes 3^-_1)_{1^-}]_{3/2^-}$ configurations is observed in the structure of the states at 3.04 MeV (8.2%) and 3.14 MeV (17.6%). In the investigated energy region, the $[2^+_1\otimes 3^-_1]_{1^-}$ component is distributed mainly over two $5/2^-$ states at 3.2 MeV (69.7%) and 4.35 MeV (14.6%). From the QPM calculations of the $1/2^-$ states, one gets two states at energies 4.34 and 4.37 MeV where the $[qp\otimes(2^+_1\otimes 3^-_1)_{1^-}]_{3/2^-}$ configurations are predominantly concentrated (22.1% and 35.2%). The structure and the corresponding widths are presented in Table XII.

In Fig. 6 the results of the calculations of the multipole strength distributions ($E1$, $M1$, and $E2$) are compared with the experimentally observed strength distribution in ^{137}Ba. A nearly quantitative agreement between the calculated $E1$ strengths and the experimental data is seen with respect to both the absolute values and the distribution pattern. The calculated total $B(E1)$ transition probability is equal to $5.2\times 10^{-3}\ e^2$ fm^2. The bump of dipole excitations observed in the experiment around about 3.8 MeV is shifted to 4.045 MeV in the calculated strength distribution. These excitations were attributed to the fragmented strength of the two-phonon excitation in ^{138}Ba at 4026 keV coupled to one quasiparticle (see Sec. V D and Table XIV).

TABLE XI. QPM calculation of the excitation energies (E) and ground-state decay widths for $E2$ and $M1$ transitions [$\Gamma_{J_i\to g.s}(E2)$ and $\Gamma_{J_i\to g.s}(M1)$] of positive parity states to the ground state ($3/2^+$) in ^{137}Ba. Only the states with $\Gamma_{J_i\to g.s}(E2)>1$ meV and $\Gamma_{J_i\to g.s}(M1)>1$ meV are presented.

$Ji\pi$	E (MeV)	α^+	α^+Q^+	$\Gamma_{J_i\to g.s}(E2)$ (meV)	$\Gamma_{J_i\to g.s}(M1)$ (meV)
$1/2^+$	1.797	$3s_{1/2}(8.2\%)$	$2d_{3/2}\otimes 2^+_1(89.7\%)$	6.96	
$1/2^+$	2.884	$3s_{1/2}(0.2\%)$	$2d_{3/2}\otimes 2^+_5(99.6\%)$	6.66	
$1/2^+$	3.223	$3s_{1/2}(<0.1\%)$	$2d_{3/2}\otimes 2^+_6(99.9\%)$	3.35	
$3/2^+$	1.687	$2d_{3/2}(1.7\%)$	$2d_{3/2}\otimes 2^+_1(95.8\%)$	6.64	
$3/2^+$	2.881	$2d_{3/2}(<0.1\%)$	$2d_{3/2}\otimes 2^+_5(99.8\%)$	6.66	
$3/2^+$	3.221	$2d_{3/2}(<0.1\%)$	$2d_{3/2}\otimes 2^+_6(98.8\%)$	3.38	
$3/2^+$	3.298	$2d_{3/2}(2.8\%)$	$1g_{7/2}\otimes 2^+_1(86.1\%)$		2.31
$5/2^+$	1.247	$2d_{5/2}(46.6\%)$	$3s_{1/2}\otimes 2^+_1(17.3\%)$		4.86
$5/2^+$	1.701	$2d_{5/2}(4.4\%)$	$2d_{3/2}\otimes 2^+_1(82.1\%)$	6.05	1.16
$5/2^+$	2.367	$2d_{5/2}(11.5\%)$	$2d_{3/2}\otimes 4^+_1(51.0\%)$		8.09
$5/2^+$	2.881	$2d_{5/2}(0.1\%)$	$2d_{3/2}\otimes 2^+_5(99.3\%)$	6.77	
$5/2^+$	3.222	$2d_{5/2}(<0.1\%)$	$2d_{3/2}\otimes 2^+_6(99.0\%)$	3.4	
$5/2^+$	3.947	$2d_{5/2}(0.9\%)$	$2d_{5/2}\otimes 2^+_1(63.8\%)$		2.73
$7/2^+$	1.175	$1g_{7/2}(51.1\%)$	$2d_{3/2}\otimes 2^+_1(39.3\%)$	1.0	
$7/2^+$	1.920	$1g_{7/2}(24.9\%)$	$2d_{3/2}\otimes 2^+_1(57.8\%)$	5.51	
$7/2^+$	2.884	$1g_{7/2}(0.2\%)$	$2d_{3/2}\otimes 2^+_5(98.1\%)$	6.8	
$7/2^+$	3.221	$1g_{7/2}(<0.1\%)$	$2d_{3/2}\otimes 2^+_6(97.9\%)$	3.3	

TABLE XII. QPM calculations of the excitation energies (E), structure, and corresponding ground-state decay widths $[\Gamma_{J_i\to g,s}(E1)]$ for $E1$ transitions of negative parity states to the ground state $(3/2^+)$ in ^{137}Ba. Only the states with $\Gamma_{J_i\to g.s}(E1)>0.1$ meV are presented. In the structure of every state the contributions of the largest α^+Q^+ component (in %) and of the all included $\alpha^+\otimes[2_1^+\otimes 3_1^-]_{1^-}$ configurations (in %) up to 4.4 MeV are given.

J_i^π	E (MeV)	α^+	α^+Q^+	$\Sigma_\alpha\alpha^+\otimes[2_1^+\otimes 3_1^-]_{1^-}$ (%)	$\Gamma_{J_i\to g,s}(E1)$ (meV)
$1/2^-$	4.045	$2p_{1/2}(0.8\%)$	$2d_{3/2}\otimes 2_1^-(91.6\%)$	4.1	177.4
$1/2^-$	4.341	$2p_{1/2}(0.6\%)$	$2p_{3/2}\otimes 2_1^+(74.5\%)$	22.1	163.8
$1/2^-$	4.371	$2p_{1/2}(0.6\%)$	$2d_{5/2}\otimes 3_1^-(62.7\%)$	35.2	156.8
$3/2^-$	2.701	$2p_{3/2}(0.1\%)$	$1h_{11/2}\otimes 4_1^+(96.1\%)$	1.7	6.95
$3/2^-$	3.040	$2p_{3/2}(0.7\%)$	$2d_{3/2}\otimes 3_1^-(82.5\%)$	8.2	7.00
$3/2^-$	3.136	$2p_{3/2}(<0.1\%)$	$1h_{11/2}\otimes 4_2^+(77.9\%)$	17.6	0.1
$3/2^-$	3.456	$2p_{3/2}(0.1\%)$	$1h_{11/2}\otimes 4_3^+(97.9\%)$	1.6	1.00
$3/2^-$	4.333	$2p_{3/2}(2.2\%)$	$2p_{1/2}\otimes 2_1^+(49.4\%)$	44.3	62.2
$5/2^-$	2.748	$1f_{5/2}(0.1\%)$	$1h_{11/2}\otimes 4_1^+(99.8\%)$	<0.1	0.4
$5/2^-$	3.134	$1f_{5/2}(0.5\%)$	$2d_{3/2}\otimes 3_1^-(73.9\%)$	10	5.8
$5/2^-$	3.210	$1f_{5/2}(0.4\%)$	$2d_{3/2}\otimes 3_1^-(24.4\%)$	69.7	4.6
$5/2^-$	4.342	$1f_{5/2}(0.2\%)$	$2p_{3/2}\otimes 2_1^+(99.5\%)$	0.2	4.5
$5/2^-$	4.348	$1f_{5/2}(0.2\%)$	$2d_{5/2}\otimes 3_1^-(85.0\%)$	14.6	6.1

C. *M*1 excitations in the even–even Ba isotopes

As can be seen in Fig. 5, no $M1$ excitations could be observed in the magic isotope ^{138}Ba (deformation parameter $\beta_2=0.093$) below 4 MeV. A magnetic dipole excitation emerges first in ^{136}Ba ($\beta_2=0.124$). However, the transition to the 1^+ level at 3370 keV has a strength of only $B(M1)\uparrow=0.17(2)\ \mu_N^2$. In the neighboring ^{134}Ba ($\beta_2=0.164$) the 1^+ state at 2939 keV is lower in energy and has an increased strength of $0.31(4)\ \mu_N^2$. It can be considered as the main fragment of the scissors mode.

Here, it should be noted that before the phase transition point to the deformed phase is reached, the "scissors mode" appears as a $J^\pi=1_{ms}^+$ two-phonon state with proton-neutron mixed-symmetry character [45–47]. Its two-phonon changing $M1$ coupling to the ground state is suppressed and the $M1$ transition rate to the symmetric two-phonon states is enhanced. Best evidence for this scheme is given by our comprehensive data on the nucleus ^{94}Mo [48,49].

The vibrational nucleus ^{136}Ba must be expected to also exhibit mixed-symmetry multiphonon structures [47]. The fundamental one-phonon $2_{1,ms}^+$ state has been discussed already in Ref. [26]. The lowest 1^+ state of ^{136}Ba at 2694 keV is short-lived [$\tau=19(4)$ fs] and indeed decays strongly to the 2_2^+ symmetric two-phonon state. Unfortunately, the $E2/M1$ multipole mixing ratio for this $1^+\to 2_2^+$ transition is unknown. Assuming it has a pure $M1$ character, the decay rate converts into a large value of $B(M1;1_{2694}^+\to 2_2^+)=0.6\ \mu_N^2$, which supports the mixed-symmetry two-phonon character of the 1^+ level at 2694 keV in ^{136}Ba.

The isotope ^{134}Ba is located closer to the critical point to the deformed phase. Here the $M1$ coupling to the ground state increases. The total $M1$ strength, which can be estimated by adding up the weaker strengths of neighboring

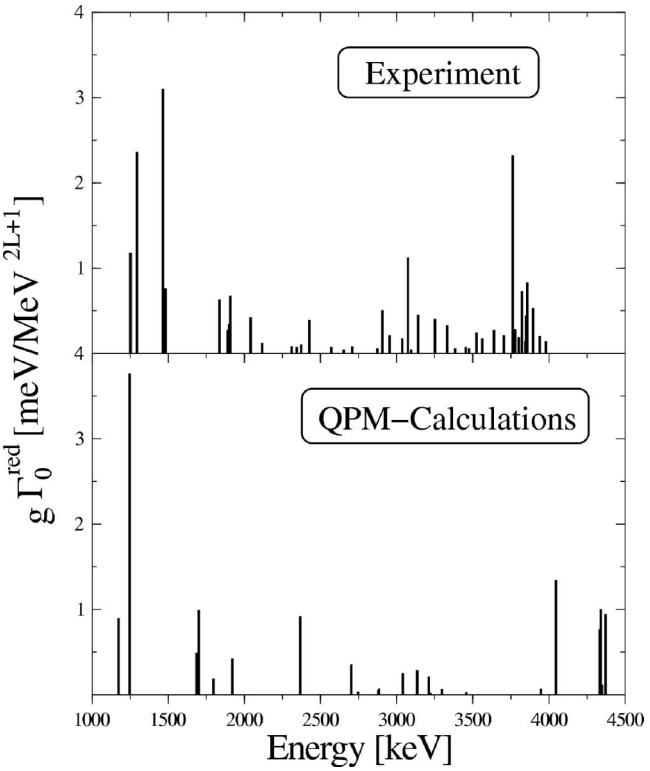

FIG. 6. Comparison of the experimentally observed multipole strength distribution ($E1$, $M1$, and $E2$) in ^{137}Ba with results of microscopic calculations in the framework of the quasiparticle-phonon model (QPM). Upper panel (a): Experimental data, for all transitions a dipole character was assumed, besides for the known $E2$ excitation at 1252 keV; lower panel: Results of the QPM calculations (see text).

TABLE XIII. $E1$ two-phonon excitations in the even–even Ba isotopes. The experimentally observed excitation energies E_{1^-} of the 1^- levels of the two-phonon quintuplet $(2^+\otimes 3^-)$ are given together with the energies of the corresponding one-phonon excitations E_{2^+}, E_{3^-} and their sums. Furthermore, the observed decay branchings R_{expt} and excitation strengths $B(E1)\uparrow$ are quoted.

Isotope	E_{1^-} (keV)	E_{2^+} (keV)	E_{3^-} (keV)	$E_{2^+}+E_{3^-}$ (keV)	R_{expt}	$B(E1)\uparrow$ $(10^{-3}\,e^2\mathrm{fm}^2)$	Ref.
^{138}Ba	4027	1436	2881	4317		11.9(13)	[57]
	4026	1436	2881	4317	$\leqslant 0.15$	13.0(28)	[27]
	4025	1436	2881	4317	0.15(4)	16.7(8)	[60]
^{136}Ba	3436	819	2532	3351	$\leqslant 0.14$[a]	6.2(14)	[57]
	3436	819	2532	3351		5.39(33)	[26]
^{134}Ba	2824	605	2255	2860	0.36(17)	2.30(30)	[25]

[a]Reference [68].

states, where a positive parity can be assumed from the measured decay branching ratios (see Ref. [25]), amounts to $B(M1)\uparrow\mathrm{tot}=0.56(4)\ \mu_N^2$. This value is in rough agreement with IBM-2 predictions in the O(6) limit [50] of $B(M1)\uparrow_{O(6)}=0.72\ \mu_N^2$. Unfortunately, the lighter stable even–even Ba isotopes ^{130,132}Ba occur only with very low natural abundances of 0.106% and 0.101%, respectively. Therefore, no enriched target samples in gram quantities were available at present for NRF experiments.

D. $E1$ two-phonon-excitation strengths in the even–even Ba isotopes ^{134,136,138}Ba and their fragmentation in the odd-mass isotopes ^{135,137}Ba

In spherical even–even nuclei near closed shells the coupling of quadrupole and octupole phonons leads to two-phonon excitations of the type $2^+\otimes 3^-$, a quintuplet of negative parity states (1^- to 5^-). The spin 1 member can ideally be investigated in photon scattering experiments. The two-phonon nature of these 1^- states has been confirmed by measurements of the branching ratios of their one-phonon decay into the 3_1^- and 2_1^+ vibrational states [51,52]. A comprehensive compilation of existing experimental NRF data and their interpretation can be found in Ref. [18].

A common feature of these $E1$ excitations, which were observed as a general phenomenon in nuclei near the shell closures $Z,N=28$; $Z,N=50$; $N=82$ [18], are excitation energies E_1 very close to the sum $(E_{2^+}+E_{3^-})$ of the corresponding one-phonon energies, suggesting a nearly harmonic coupling. The reduced transition probabilities for the ground-state decays $B(E1)\downarrow$ are maximal at the corresponding magic number. These values gradually decrease with increasing distance to the shell closure. The opposite is observed for the decay of the 1^- states to the first excited 2_1^+ one-phonon states. The $B(E1,1_1^-\rightarrow 2_1^+)$ values are generally lowest at magic numbers. They increase when leaving the shell closure, with some irregularities. This behavior could be explained on the basis of the QPM as due to the dipole core polarization associated with the electric giant dipole resonance (GDR) [18].

The experimental data for the $E1$ two-phonon excitations in ^{134,136,138}Ba fit nicely into the systematics. The numerical results are summarized in Table XIII and depicted in graphical form in Fig. 7. In the upper part are plotted the energies of the 2_1^+ (open squares), 3_1^- (open diamonds) one-phonon excitations, and the observed 1^- two-phonon excitations (full crosses). They are compared to the expected sum energies $\Sigma=E_{2^+}+E_{3^-}$ (open hexagons). In the lower part the experimental $B(E1)\uparrow$ values for the two-phonon excitations are shown. Obviously, the strengths drastically decrease when leaving the magic number $N=82$. A similar effect was observed in nuclei with additional neutrons outside the $N=82$ shell, where more experimental data are available. The Ba isotopic chain has one of the rare possibilities to study the influence of neutron holes on the dipole strength distribu-

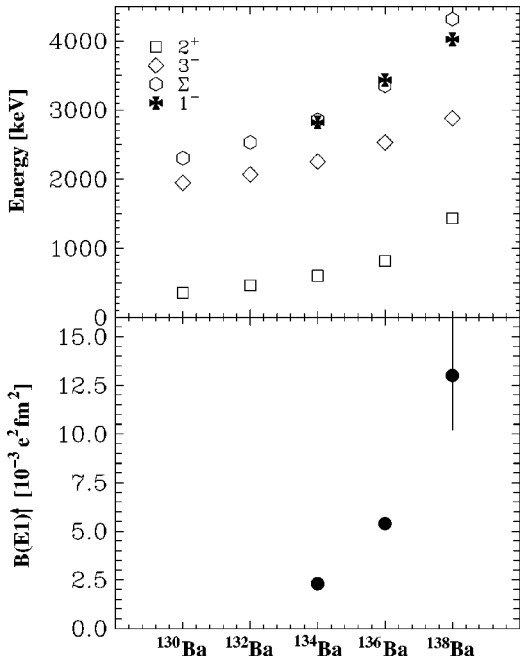

FIG. 7. Systematics of $E1$ two-phonon excitations in the even–even Ba isotopes. Upper part: Energies of the 2_1^+ (open squares), 3_1^- (open diamonds) one-phonon excitations and of the observed 1^- two-phonon excitations (full crosses) in ^{134,136,138}Ba compared to the expected sum energies $\Sigma=E_{2^+}+E_{3^-}$ (open hexagons). Lower part: Experimental $B(E1)\uparrow$ values for the two-phonon excitations (full symbols). Error bars are smaller than the size of the symbols if not explicitly depicted.

TABLE XIV. Comparison of experimental data for the $E1$ two-phonon–particle strengths in odd-mass nuclei near the shell closure $N=82$ with the two-phonon strengths in the neighboring even–even core nuclei. For both, the odd-mass isotopes and the corresponding even–even core nuclei the proton and neutron numbers Z,N are given for comparison.

Isotope	Z	N	$\Sigma B(E1)\uparrow$ (10^{-3} e^2fm^2)	Ref.	Core	Z_C	N_C	$B(E1)\uparrow$ (10^{-3} e^2fm^2)	Ref.
^{135}Ba	56	79	2.1±0.3[a]	This work	^{134}Ba	56	78	2.3±0.3	[25]
			4.5±0.6[b]	This work	^{136}Ba	56	80	5.39±0.33	[26]
^{137}Ba	56	81	6.0±0.6	This work	^{138}Ba	56	82	13.0±2.8	[27]
^{139}La	57	82	6.6±0.7	[64]	^{138}Ba	56	82	13.0±2.8	[27]
					^{140}Ce	58	82	16.7±0.8	[27]
^{141}Pr	59	82	7.1±1.9	[64]	^{140}Ce	58	82	16.7±0.8	[27]
					^{142}Nd	60	82	16.3±2.4	[21]
^{143}Nd	60	83	13.6±1.8	[62,63]	^{142}Nd	60	82	16.3±2.4	[21]
					^{144}Sm	62	82	18.8±2.6	[65,66]

[a]Assuming the same $E1/M1$ ratio as in ^{134}Ba, see text and Ref. [67].
[b]Assuming the same $E1/M1$ ratio as in ^{136}Ba, see text and Ref. [67].

tions. Another very interesting chain for such studies represent the Xe isotopes with seven stable even–even isotopes from ^{136}Xe ($N=82$) down to ^{124}Xe. The corresponding first photon scattering experiments on these nuclei were already started successfully at Stuttgart [53].

Fundamental low-lying dipole modes in heavy nuclei, like the $M1$ scissors mode and the $E1$ two-phonon excitations, have mostly been studied in even–even nuclei. The fragmentation of these modes in the neighboring odd-mass nuclei is of interest, since it may provide information on the interplay between the coupling of these rather collective modes with particle or hole degrees of freedom.

The longstanding puzzle of the missing scissors mode strengths in odd-mass rare earth nuclei could recently be resolved by improved photon scattering experiments and statistical fluctuation analyses [58,59] of the spectra of scattered photons (see Ref. [54] and references therein). The $M1$ dipole strength distributions are generally extremely fragmented, with the exception of ^{163}Dy. Recent results demonstrate that the amount of dipole strength experimentally observed is very sensitive to the experimental energy resolution and the overall detection limits.

In the case of the two-phonon excitations in the odd-mass neighbors of magic even–even nuclei experimental data exist for nuclei near the $Z=50$ shell closure. The coupling of an additional proton to the $Z=50$ core was studied in NRF experiments on ^{121,123}Sb [55]. Corresponding data exist for ^{115}In ($Z=49$, one proton hole) [56]. Whereas in ^{115}In and ^{121}Sb the integrated strengths nearly reach those of the two-phonon excitations in the core nuclei, in ^{123}Sb only half of the expected strength could be detected (see Ref. [55]). Near the $N=82$ shell closure the odd-mass isotope ^{143}Nd was studied extensively [62,63]. Here the coupling of the $f_{7/2}$ neutron outside the closed shell to the quintuplet of two-phonon excitations leads to a fragmentation of the $E1$ strength. The experimentally observed integrated $E1$ strengths are comparable to that of the 1^- member of the two-phonon quintuplet in the core nucleus ^{142}Nd. Furthermore, the strength distribution pattern could be reproduced by calculations in the framework of a weak particle-core coupling model [62,63]. On the other hand, there were no experiments up to now studying the coupling of neutron holes to the core excitations. Therefore, the present experiments on ^{137,135}Ba are of special interest.

In Table XIV the total dipole strengths in the odd-mass Ba isotopes ^{135,137}Ba are summarized. Since in these nearly spherical nuclei $M1$ scissors mode strength should be negligible and $E2$ excitations in NRF are rather suppressed, the observed total strengths are ascribed to the fragmented $E1$ strengths of the two-phonon excitations. The data are compared to the $B(E1)\uparrow$ values measured for the two-phonon excitations in even–even core nuclei and the neighboring $N=82$ isotones ^{139}La and ^{141}Pr. The integration limits for the strengths in ^{135,137}Ba were properly chosen according to the energy ranges of the corresponding excitations in the core nuclei ^{134,136,138}Ba (compare Fig. 5). Furthermore, since no parities could be determined for the dipole excitations in ^{135,137}Ba, the same $E1/M1$ strength ratios were assumed as found in the core nuclei as a crude estimation.

As can be seen, the total $E1$ strengths in ^{135}Ba deduced in this manner strongly depend on the choice of the corresponding core. However, it is nearly the same as compared to that in the chosen neighboring core nuclei ^{134}Ba or ^{136}Ba with their different $E1/M1$ ratios. In any case, the detected total dipole strength observed in ^{135}Ba is more fragmented as compared to ^{137}Ba. This trend of an increasing fragmentation of the dipole strength with decreasing mass number A is continued as documented by the results for ^{133}Cs ($Z=55$, $N=78$), where numerous, but only very weak dipole excitations could be detected [61].

The observed strength in ^{137}Ba is only about one half of that in ^{138}Ba where no $M1$ excitations were detected in the relevant energy range. A trivial reason for this reduction might be the fact that the two-phonon excitation in ^{138}Ba is at 4026 keV and some of the fragments of the two-phonon-hole states in ^{137}Ba may be shifted to higher energies (as suggested by the QPM calculations, see Table XII), which were not accessible in the Stuttgart experiment due to the energy

limitations of the Dynamitron accelerator. However, the $E1$ strength in ^{137}Ba is the same as in the lighter core nucleus ^{136}Ba. A similar result is found for the two-phonon-particle states in ^{143}Nd, where almost the same strength is recovered as that of the two-phonon states in the even–even $N=82$ isotones ^{142}Nd and ^{144}Sm. The situation seems to be different in the odd-mass $N=82$ isotones ^{139}La and ^{141}Pr with midshell valence protons where only about one half of the $E1$ strength as in the even–even $N=82$ isotones could be detected. To what extent this is only due to a poorer sensitivity in these older NRF experiments [64] must be clarified by future improved measurements.

E. The dipole strength distributions in the stable Ba isotopes in view of the new critical point symmetries

In Fig. 8 the reduced transition probabilities $B(E2)\uparrow$ for the excitation of the first 2^+ states in the stable even–even nuclei within the Xe, Ba, Nd, Sm, and Gd isotopic chains are plotted as a function of the neutron number N. The $B(E2)\uparrow$ values are, as well known, proportional to the squares of the deformation parameters β_2 [69]. As to be seen clearly in Fig. 8 $B(E2)\uparrow$ is minimum, as expected, for the magic nuclei with neutron number $N=82$. For the neutron-rich nuclei with $N\geqslant 82$ a universal increase of the $B(E2)\uparrow$ values with rising neutron numbers can be stated for all isotopic chains reaching some saturation above $N\geqslant 92$. In particular, near $N=90$ a sudden jump in the deformation, corresponding to large $B(E2)\uparrow$ values, is obvious. The $N=90$ isotones ^{154}Gd, ^{152}Sm, and ^{150}Nd are exactly the proposed $X(5)$ candidates. The sudden onset of the deformation causes an abrupt opening of the deformation splitting of the GDR, as nicely documented by photoneutron cross-section measurements on nuclei of the Nd and Sm isotopic chains [8,9]. The sudden shape transition is visibly more pronounced than in Fig. 8 when plotting the $B(E2)\uparrow$ values as a function of the so-called Casten $\mathcal{P}$ factor [70]. $\mathcal{P}$ is defined as $\mathcal{P}=N_p\cdot N_n/(N_p+N_n)$ where N_p and N_n are the number of protons and neutrons outside a closed shell, respectively [71]. In this presentation the $B(E2)\uparrow$ values follow a step-like function where the steep increase lies at critical $\mathcal{P}$-parameters of $\mathcal{P}_{\mathrm{crit}}\approx 4-5$, exactly in the region of the $N=90$ isotones, the $X(5)$ candidates. The same behavior was found for the total $M1$ scissors mode strengths [70]. The underlying proportionality between the $B(E2)\uparrow$ and the total $M1$ scissors mode strengths was observed experimentally [72] and explained theoretically [73,74]. For these nuclei a sudden concentration of the scissors mode excitations in a narrow energy range around 3 MeV is obvious [21–23,19,20]. It is further remarkable that for each isotopic chain the mean excitation energy of the scissors mode, i.e., the center of gravity of the $M1$ excitation strength distribution, seems to be lowest for the critical point nuclei. This can be obtained from the data on the Sm and Nd isotopic sequences that include the $N=90$ critical point nuclei [15]. To what extent this is a general phenomenon must be left at this point to future investigations.

Also in the low-lying electric dipole distributions pronounced changes can be seen. The systematics of low-lying

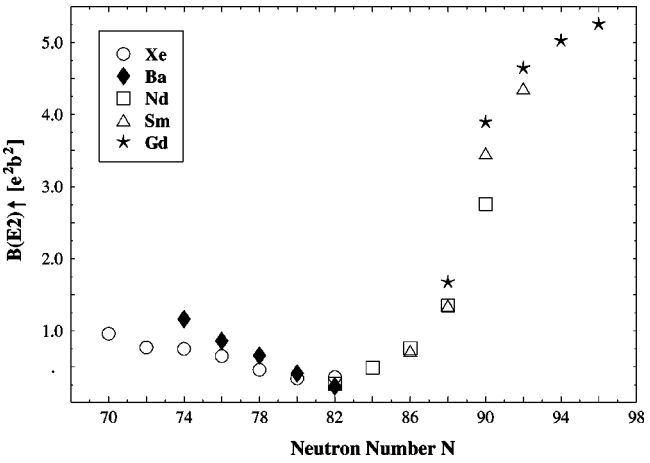

FIG. 8. Reduced transition probabilities $B(E2)\uparrow$, which are proportional to the squares of the deformation parameters β_2, as a function of the neutron number N for the stable even–even nuclei of the Xe, Ba, Nd, Sm, and Gd isotopic chains. All data are taken from a recent compilation by Raman *et al.* [69].

$E1$ excitations in nuclei of the mass region $A=130-200$ was summarized and discussed in a recent article by Fransen *et al.* [75]. Two features are remarkable. First, the excitation energy of the lowest 1^- state is lowest for the $N=90$ isotones; secondly, the excitation strength $B(E1)\uparrow$ has a minimum around $N=84$ and jumps at $N=90$ to a saturation value which is as high as the values for the strong $E1$ two-phonon excitations in the closed shell nuclei ($N=82$).

To summarize, the first order phase transition from spherical to deformed shapes can be observed besides in the systematics of the often discussed excitation energy ratios E_{4^+}/E_{2^+} and $B(E2)$ values also in the dipole strength distributions of neutron rich nuclei above $N=82$. It can be seen in the shape of the high-lying electric giant dipole resonance (GDR), in the $M1$ scissors mode strength distribution, but also in the low-lying electric dipole strength systematics.

The situation for the neutron-deficient nuclei with neutron numbers $N\leqslant 82$ is quite different. The $B(E2)\uparrow$ values increase linearly with decreasing neutron number N as shown for the Ba and Xe isotopic chains in Fig. 8. In an extended systematics, including unstable even-even nuclei of the Sn, Te, Xe, Ba, Ce, and Nd isotopic chains, Dewald [76] demonstrated that for all these isotopes the $B(E2)\uparrow$ values increase linearly with dropping neutron number N, however, with different slopes. For the isotopes with higher proton number Z steeper slopes were observed. This behavior is distinctly different from the findings for the neutron-rich isotopes, where the $B(E2)\uparrow$ values fall on one universal curve for all isotopes and increase nonlinearly with an abrupt jump.

Unfortunately, for the neutron deficient nuclei $E1$ GDR-data exist only for the spherical Sn-isotopes ^{116,118,120,124}Sn [77] and the vibrator nuclei ^{124,126,128,130}Te [78] exhibiting a deformation splitting not at all corresponding to the small $B(E2)$ values. In addition, the even-even Sn isotopes show a remarkably uniform low-lying $E1$ strength distribution. The $E1$ strengths are concentrated in the two-phonon excitations with nearly constant $B(E1)\uparrow$ values [79].

For the Ba isotopic chain, where ^{134}Ba was proposed as an $E(5)$ candidate [4], the $E1$ GDR photoabsorption cross

section was only measured for the magic isotope ^{138}Ba ($N=82$) [80]. The shape of this cross section is nicely described by one Lorentzian, as expected for a spherical nucleus. Not a single one of the numerous neighboring stable Xe isotopes was studied in the energy range of the GDR due to the experimental problems with enriched gaseous targets of gram quantities (see [81]). Therefore, the discussion of the dipole strength distributions up to now has been restricted to the few data on low-lying dipole excitations in ^{134,136,138}Ba presented in this paper.

In Fig. 5 the observed dipole strength distributions are depicted. The $M1$ scissors mode excitation emerges in ^{136}Ba as a mixed-symmetry two-phonon state and increases with deformation. In the $E(5)$ candidate ^{134}Ba the total $M1$ strength amounts to about $\Sigma B(M1)\uparrow = 0.56(4)\ \mu_N^2$, comparable to that in the O(6) representative ^{196}Pt [82]. The increase of the strength and the shift in energy are rather smooth.

The data on the $E1$ two-phonon excitations in the even-even Ba isotopes are summarized in Table XIII. The strong $E1$ two-phonon excitation in ^{138}Ba exhausts the complete low-lying $E1$ strength in this nucleus. This excitation is shifted to lower energies nearly linearly when moving to the lighter isotopes ^{136,134}Ba. The strength is reduced rather dramatically (see Fig. 7). Such a behavior is not observed for nuclei with $N \geqslant 82$ (see [18]).

Obviously, for a detailed discussion of possible signatures for a second order phase transition when approaching ^{134}Ba the data basis is too sparse. Up to now the other two existing stable Ba isotopes ^{132,130}Ba could not be studied in NRF experiments. Due to their low natural abundance, enriched targets in gram quantities are unaffordably expensive. On the other hand, the Xe isotopic chain ($Z=54$) with seven stable even-even isotopes is also very interesting to study, since it reaches from the $N=82$ isotope ^{136}Xe down to the $N=70$ isotope ^{124}Xe. However, the gaseous nature of xenon represents an experimental challenge. Fortunately, it could be overcome by the development of high pressure gas-targets at FZ-Karlsruhe [83]. First NRF experiments performed at the Stuttgart bremsstrahlung facility on ^{124,128,130,132,134}Xe showed encouraging results [53].

ACKNOWLEDGMENTS

The financial support of the Stuttgart projects by the Deutsche Forschungsgemeinschaft (DFG) (Contract Nos. Kn 154/30,31 and Br799/11) and by the Bulgarian Science Foundation (Contract No. 1311) is gratefully acknowledged. N.P. thanks the NSF for support under Grant No. PHY 0245018. The authors are indebted to Tan Ahn for his critical and careful reading of the manuscript.

[1] F. Iachello, Phys. Rev. Lett. **85**, 3580 (2000).
[2] F. Iachello, Phys. Rev. Lett. **87**, 052502 (2001).
[3] F. Iachello, Phys. Rev. Lett. **91**, 132502 (2003).
[4] R. F. Casten and N. V. Zamfir, Phys. Rev. Lett. **85**, 3584 (2000).
[5] R. F. Casten and N. V. Zamfir, Phys. Rev. Lett. **87**, 052503 (2001).
[6] R. Krücken, B. Albanna, C. Bialik, R. F. Casten, J. R. Cooper, A. Dewald, N. V. Zamfir, C. J. Barton, C. W. Beausang, M. A. Caprio, A. A. Hecht, T. Klug, J. R. Novak, N. Pietralla, and P. von Brentano, Phys. Rev. Lett. **88**, 232501 (2002).
[7] R. Bijker, R. F. Casten, N. V. Zamfir, and E. A. McCutchan, Phys. Rev. C **68**, 064304 (2003).
[8] P. Carlos, H. Beil, R. Bergère, A. Leprêtre, A. de Miniac, and A. Veyssière, Nucl. Phys. **A225**, 171 (1974).
[9] P. Carlos, H. Beil, R. Bergère, A. Leprêtre, and A. Veyssière, Nucl. Phys. **A172**, 437 (1971).
[10] J. E. Garcìa-Ramos, J. M. Arias, J. Barea, and A. Frank, Phys. Rev. C **68**, 024307 (2003).
[11] U. Kneissl, H. H. Pitz, and A. Zilges, Prog. Part. Nucl. Phys. **37**, 349 (1996).
[12] N. Lo Iudice and F. Palumbo, Phys. Rev. Lett. **41**, 1532 (1978).
[13] D. Bohle, A. Richter, W. Steffen, A. E. L. Dieperink, N. Lo Iudice, F. Palumbo, and O. Scholten, Phys. Lett. **137B**, 27 (1984).
[14] A. Richter, Prog. Part. Nucl. Phys. **34**, 261 (1995).
[15] N. Pietralla, P. von Brentano, R.-D. Herzberg, U. Kneissl, N. Lo Iudice, H. Maser, H. H. Pitz, and A. Zilges, Phys. Rev. C **58**, 184 (1998).
[16] D. Zawischa, J. Phys. G **24**, 683 (1998).
[17] N. Lo Iudice, Riv. Nuovo Cimento **23**, 1 (2000).
[18] W. Andrejtscheff, C. Kohstall, P. von Brentano, C. Fransen, U. Kneissl, N. Pietralla, and H. H. Pitz, Phys. Lett. B **506**, 239 (2001).
[19] W. Ziegler, C. Rangacharyulu, A. Richter, and C. Spieler, Phys. Rev. Lett. **65**, 2515 (1990).
[20] W. Ziegler, N. Huxel, P. von Neumann-Cosel, C. Rangacharyulu, A. Richter, C. Spieler, C. De Coster, and K. Heyde, Nucl. Phys. **A564**, 366 (1993).
[21] H. H. Pitz, R. D. Heil, U. Kneissl, S. Lindenstruth, U. Seemann, R. Stock, C. Wesselborg, A. Zilges, P. von Brentano, S. D. Hoblit, and A. M. Nathan, Nucl. Phys. **A509**, 587 (1990).
[22] J. Margraf, R. D. Heil, U. Kneissl, U. Maier, H. H. Pitz, H. Friedrichs, S. Lindenstruth, B. Schlitt, C. Wesselborg, P. von Brentano, R.-D. Herzberg, and A. Zilges, Phys. Rev. C **47**, 1474 (1993).
[23] T. Eckert, O. Beck, J. Besserer, P. von Brentano, R. Fischer, R.-D. Herzberg, U. Kneissl, J. Margraf, H. Maser, A. Nord, N. Pietralla, H. H. Pitz, S. W. Yates, and A. Zilges, Phys. Rev. C **56**, 1256 (1997); **57**, 1007 (1998).
[24] R. F. Casten and P. von Brentano, Phys. Lett. **152B**, 22 (1985).
[25] H. Maser, N. Pietralla, P. von Brentano, R.-D. Herzberg, U. Kneissl, J. Margraf, H. H. Pitz, and A. Zilges, Phys. Rev. C **54**, R2129 (1996).
[26] N. Pietralla, D. Belic, P. von Brentano, C. Fransen, R.-D. Herzberg, U. Kneissl, H. Maser, P. Matschinsky, A. Nord, T. Otsuka, H. H. Pitz, V. Werner, and I. Wiedenhöver, Phys. Rev.

C **58**, 796 (1998).
[27] R.-D. Herzberg, I. Bauske, P. von Brentano, Th. Eckert, R. Fischer, W. Geiger, U. Kneissl, J. Margraf, H. Maser, N. Pietralla, H. H. Pitz, and A. Zilges, Nucl. Phys. **A592**, 211 (1995).
[28] Yu. P. Gangrskiĭ, A. P. Tonchev, and N. P. Balabanov, Phys. Part. Nucl. **27**, 426 (1996).
[29] J. J. Carroll, C. B. Collins, K. Heyde, M. Huber, P. von Neumann-Cosel, V. Yu. Ponomarev, D. G. Richmond, A. Richter, C. Schlegel, T. W. Sinor, and K. N. Taylor, Phys. Rev. C **48**, 2238 (1993).
[30] D. Belic, J. Besserer, C. Arlandini, J. de Boer, J. J. Carroll, J. Enders, T. Hartmann, F. Käppeler, H. Kaiser, U. Kneissl, M. Loewe, H. Maser, P. Mohr, P. von Neumann-Cosel, A. Nord, H. H. Pitz, A. Richter, M. Schumann, S. Volz, and A. Zilges, Nucl. Instrum. Methods Phys. Res. A **463**, 26 (2001).
[31] U. Kneissl, BgNS Trans. **7**, 33 (2002).
[32] U. E. P. Berg and U. Kneissl, Annu. Rev. Nucl. Part. Sci. **37**, 33 (1987).
[33] F. Stedile *et al.* (unpublished).
[34] V. A. Bondarenko, I. L. Kuvaga, P. T. Prokofjev, V. A. Khitrov, Yu. V. Kholnov, Le Hong Khiem, Yu. P. Popov, A. M. Sukhovoj, S. Brant, V. Paar, and V. Lopac, Nucl. Phys. **A551**, 54 (1993).
[35] Yu. V. Sergeenkov and B. Singh, Nucl. Data Sheets **84**, 115 (1998).
[36] V. A. Bondarenko, I. L. Kuvaga, P. T. Prokofjev, A. M. Sukhovoj, V. A. Khitrov, Yu. P. Popov, S. Brant, and V. Paar, Nucl. Phys. **A582**, 1 (1995).
[37] J. K. Tuli, Nucl. Data Sheets **81**, 579 (1997).
[38] E. Drăgulescu, M. Ivaşcu, R. Mihu, D. Popescu, G. Semenescu, A. Velenik, and V. Paar, J. Phys. G **10**, 1099 (1984).
[39] V. G. Soloviev, *Theory of Atomic Nuclei: Quasiparticles and Phonons* (Institute of Physics, Bristol, 1992).
[40] S. Gales, Ch. Stoyanov, and A. I. Vdovin, Phys. Rep. **166**, 125 (1988).
[41] Ch. Stoyanov and C. Q. Khuong, JINR Dubna Report P4-81-234 (1981) (unpublished).
[42] V. Yu. Ponomarev, Ch. Stoyanov, N. Tsoneva, and M. Grinberg, Nucl. Phys. **A635**, 470 (1998).
[43] M. Grinberg and Ch. Stoyanov, Nucl. Phys. **A573**, 231 (1994).
[44] J. K. Tuli, Nucl. Data Sheets **69**, 69 (1993).
[45] F. Iachello and A. Arima, *The Interacting Boson Model* (Cambridge University Press, Cambridge, 1987).
[46] N. Lo Iudice and Ch. Stoyanov, Phys. Rev. C **62**, 047302 (2000).
[47] N. Lo Iudice and Ch. Stoyanov, Phys. Rev. C **65**, 064304 (2002).
[48] N. Pietralla, C. Fransen, D. Belic, P. von Brentano, C. Friessner, U. Kneissl, A. Linnemann, A. Nord, H. H. Pitz, T. Otsuka, I. Schneider, V. Werner, and I. Wiedenhöver, Phys. Rev. Lett. **83**, 1303 (1999).
[49] C. Fransen, N. Pietralla, Z. Ammar, D. Bandyopadhyay, N. Boukharouba, P. von Brentano, A. Dewald, J. Gableske, A. Gade, J. Jolie, U. Kneissl, S. R. Lesher, A. F. Lisetzkiy, M. T. McEllistrem, M. Merrick, H. H. Pitz, N. Warr, V. Werner, and S. W. Yates, Phys. Rev. C **67**, 024307 (2003).
[50] P. van Isacker, K. Heyde, J. Jolie, and A. Sevrin, Ann. Phys. (N.Y.) **171**, 253 (1986).
[51] M. Wilhelm, E. Rademacher, A. Zilges, and P. von Brentano, Phys. Rev. C **54**, R449 (1996).
[52] M. Wilhelm, S. Kasemann, G. Pacovici, E. Rademacher, P. von Brentano, and A. Zilges, Phys. Rev. C **57**, 577 (1998).
[53] H. von Garrel, P. von Brentano, C. Fransen, A. Gade, J. Jolie, F. Käppeler, L. Käubler, U. Kneissl, C. Kohstall, A. Linnemann, N. Pietralla, H. H. Pitz, G. Rusev, M. Scheck, K. D. Schilling, R. Schwengner, F. Stedile, S. Walter, V. Werner, and K. Wisshak, Bulgarian Nuclear Society Transactions, in press (2003), and H. von Garrel, Dissertation, Stuttgart University (in preparation).
[54] A. Nord, J. Enders, A. E. de Almeida Pinto, D. Belic, P. von Brentano, C. Fransen, U. Kneissl, C. Kohstall, A. Linnemann, P. von Neumann-Cosel, N. Pietralla, H. H. Pitz, A. Richter, F. Stedile, and V. Werner, Phys. Rev. C **67**, 034307 (2003).
[55] J. Bryssinck, L. Govor, F. Bauwens, D. Belic, P. von Brentano, D. De Frenne, C. Fransen, A. Gade, E. Jacobs, U. Kneissl, C. Kohstall, A. Linnemann, A. Nord, N. Pietralla, H. H. Pitz, M. Scheck, F. Stedile, and V. Werner, Phys. Rev. C **65**, 024313 (2002).
[56] P. von Neumann-Cosel, A. Richter, C. Spieler, W. Ziegler, J. J. Carroll, T. W. Sinor, D. G. Richmond, K. N. Taylor, C. B. Collins, and K. Heyde, Phys. Lett. B **266**, 9 (1991).
[57] F. R. Metzger, Phys. Rev. C **18**, 2138 (1978).
[58] J. Enders, N. Huxel, P. von Neumann-Cosel, and A. Richter, Phys. Rev. Lett. **79**, 2010 (1997).
[59] J. Enders, N. Huxel, U. Kneissl, P. von Neumann-Cosel, H. H. Pitz, and A. Richter, Phys. Rev. C **57**, 996 (1998).
[60] R.-D. Herzberg, C. Fransen, P. von Brentano, J. Eberth, J. Enders, A. Fitzler, L. Käubler, H. Kaiser, P. von Neumann-Cosel, N. Pietralla, V. Yu. Ponomarev, H. Prade, A. Richter, H. Schnare, R. Schwengner, S. Skoda, H. G. Thomas, H. Tiesler, D. Weishaar, and I. Wiedenhöver, Phys. Rev. C **60**, 051307 (1999).
[61] J. Besserer, O. Beck, P. von Brentano, T. Eckert, R.-D. Herzberg, D. Jäger, U. Kneissl, J. Margraf, H. Maser, A. Nord, N. Pietralla, H. H. Pitz, and A. Zilges, Phys. Rev. C **56**, 1276 (1997).
[62] A. Zilges, R.-D. Herzberg, P. von Brentano, F. Dönau, R. D. Heil, R. V. Jolos, U. Kneissl, J. Margraf, H. H. Pitz, and C. Wesselborg, Phys. Rev. Lett. **70**, 2880 (1993).
[63] R.-D. Herzberg, A. Zilges, A. M. Oros, P. von Brentano, U. Kneissl, J. Margraf, H. H. Pitz, and C. Wesselborg, Phys. Rev. C **51**, 1226 (1995).
[64] R.-D. Herzberg, Dissertation, University of Cologne, 1995.
[65] F. R. Metzger, Phys. Rev. C **14**, 543 (1976).
[66] F. R. Metzger, Phys. Rev. C **17**, 939 (1978).
[67] M. Scheck, Dissertation, University of Stuttgart, in preparation.
[68] A. A. Sonzogni, Nucl. Data Sheets **95**, 837 (2002).
[69] S. Raman, C. W. Nestor, Jr., and P. Tikkanen, At. Data Nucl. Data Tables **78**, 1 (2001).
[70] C. Rangacharyulu, A. Richter, H. J. Wörtche, W. Ziegler, and R. F. Casten, Phys. Rev. C **43**, R949 (1991).
[71] R. F. Casten, D. S. Brenner, and P. E. Haustein, Phys. Rev. Lett. **58**, 658 (1987).
[72] N. Pietralla, P. von Brentano, R.-D. Herzberg, U. Kneissl, J. Margraf, H. Maser, H. H. Pitz, and A. Zilges, Phys. Rev. C **52**, R2317 (1995).
[73] K. Heyde and C. De Coster, Phys. Rev. C **44**, R2262 (1991).
[74] P. von Neumann-Cosel, J. N. Ginocchio, H. Bauer, and A.

Richter, Phys. Rev. Lett. **75**, 4178 (1995).
[75] C. Fransen, O. Beck, P. von Brentano, T. Eckert, R.-D. Herzberg, U. Kneissl, H. Maser, A. Nord, N. Pietralla, H. H. Pitz, and A. Zilges, Phys. Rev. C **57**, 129 (1998).
[76] A. Dewald, Prog. Part. Nucl. Phys. **28**, 409 (1992).
[77] A. Leprêtre, H. Beil, R. Bergère, P. Carlos, A. de Miniac, A. Veyssière, and K. Kernbach, Nucl. Phys. **A219**, 39 (1974).
[78] A. Leprêtre, H. Beil, R. Bergère, P. Carlos, J. Fagot, A. de Miniac, A. Veyssière, and H. Miyase, Nucl. Phys. **A258**, 350 (1976).
[79] J. Bryssinck, L. Govor, D. Belic, F. Bauwens, O. Beck, P. von Brentano, D. De Frenne, T. Eckert, C. Fransen, K. Govaert, R.-D. Herzberg, E. Jacobs, U. Kneissl, H. Maser, A. Nord, N. Pietralla, H. H. Pitz, V. Yu. Ponomarev, and V. Werner, Phys. Rev. C **59**, 1930 (1999).
[80] B. L. Berman, S. C. Fultz, J. T. Caldwell, M. A. Kelly, and S. S. Dietrich, Phys. Rev. C **2**, 2318 (1970).
[81] S. S. Dietrich and B. L. Berman, At. Data Nucl. Data Tables **38**, 199 (1988).
[82] P. von Brentano, J. Eberth, J. Enders, L. Esser, R.-D. Herzberg, N. Huxel, H. Meise, P. von Neumann-Cosel, N. Nicolay, N. Pietralla, H. Prade, J. Reif, A. Richter, C. Schlegel, R. Schwengner, S. Skoda, H. G. Thomas, I. Wiedenhöver, G. Winter, and A. Zilges, Phys. Rev. Lett. **76**, 2029 (1996).
[83] R. Reifarth, M. Heil, F. Käppeler, F. Voss, K. Wisshak, F. Bečvář, M. Krtička, R. Gallino, and Y. Nagai, Phys. Rev. C **66**, 064603 (2002).